HU ISSN 1785-6892 in print
HU ISSN 2064-7522 online

DESIGN OF MACHINES AND STRUCTURES

A Publication of the University of Miskolc

Volume 11, Number 2

Miskolc University Press
2021

EDITORIAL BOARD

CONTENTS

Design of Machines and Structures, Vol. 11, No. 2 (2021), pp. 5–13.
https://doi.org/10.32972/dms.2021.009
http://orcid.org/0000-0003-3207-5501 (P. Ficzere)

POTENTIAL APPLICATIONS OF ADDITIVE MANUFACTURING TECHNOLOGIES IN THE VEHICLE INDUSTRY

HUSSEIN ALZYOD – PETER FICZERE

Budapest University of Technology and Economics,
H-1111 Budapest Műegyetem rkp. 3
hussein.alzyod@edu.bme.hu, ficzere.peter@kjk.bme.hu

Abstract: One of the most competitive fields on the planet is the automotive industry. Newmarket and innovative designs regularly arise, necessitating the development of new manufacturing methods to keep up with the automotive industry. Additive manufacturing offers a significant competitive advantage in this industry, serving as a disruptive strategy by increasing production flexibility, reducing product development time, and providing optimal automotive components and bespoke vehicle products on demand. Additive manufacturing on soft assembly tools or specialised tools to make automotive components enhances automotive production. Additive Manufacturing's freeform capability allows for the design and direct fabrication of optimised automotive components aimed at improving vehicle performance, as well as tailored assembly tools to boost productivity. Another related technological advantage of additive manufacturing is the ability to create lightweight components with the help of generative design algorithms. Furthermore, the time to market for Additive Manufacturing parts has fallen dramatically, allowing mass customisation to become a reality. The strong downward trend in fuel consumption offers new automobile design, performance, and compliance with regulations. Considering the actual example switch from the conventional combustion engine to other motion systems, Additive Manufacturing is a critical enabler technology for modern automobiles. This paper provides an overview of Additive Manufacturing applications in the automobile sector, focusing on the technical and economic benefits of this manufacturing technology.

Keywords: *Additive Manufacturing (AM), Automotive, Potential Application*

1. INTRODUCTION

Additive manufacturing (AM), often known as 3D printing, is a type of production in which materials are added layer by layer. Joining substances together by binding them together layer by layer to construct intricate 3D structures is called. As the name implies, Additive Manufacturing's a way of producing lighter and stronger 3D designs by including raw material rather than removing it [1]–[5]. 3D printing is a method of manufacturing three-dimensional physical models using 3D computer-aided design (CAD). Directed energy deposition, Vat photopolymerisation, sheet lamination, material jetting, binder jetting, powder bed fusion, and material extrusion

are the seven different types of AM, as shown in *Figure 1* [6]. The 3D printer interprets the digital supply parameters obtained from the Stereolithography (STL) file format and converts them to G-codes utilising slicing tools [7].

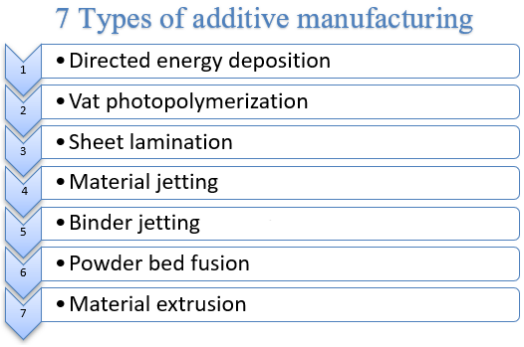

Figure 1
Classification of additive manufacturing [6]

Complex structure design and production and customisation, reuse, and improvement are all possible with this printing process. This needed cutting-edge processes like Stereo Lithography (SLA), which uses lasers to decompose photopolymer resins layer by layer. Selective Laser Sintering (SLS) is a sintered material coating method that uses a laser as a source of energy and focuses it on points in space defined by a three-dimensional object. Fused Deposition Modelling (FDM) is a process that involves heating and depositing a flexible thermoplastic filament from a long-coiled wire onto an object.

Digital Light Processing (DLP) is a method of printing three-dimensional (3D) structures created in 3D CAD software by projecting the material one layer-by-layer. It is employed in a variety of embedded systems, including medicine, automobile, and the military.

Selective Laser Melting (SLM) fuses metallic powders with high-power density lasers. Electron Beam Melting (EBM) is a prototype technology in which powder is deposited in thin layers before heated and melted. Laminated Object Manufacturing (LOM) is a cheap and fast way to make objects. The material is coated with an adhesive layer, then melted by a feeder roller before being sliced into the required shapes.

Unlike conventional manufacturing methods, which had a variety of limits on product design, AM's adaptability allows producers to fine-tune lean production tactics by minimising waste created by material removal. 3D printing has attracted the public's and specialists' attention in various fields, including automotive, aviation, industry, medicine, and food supply chain management.

AM is a truly breakthrough technology that is developing in the manufacturing branch, as leading industries switch from traditional to modern production. In AM, three-dimensional 3D printing is utilised to switch engineering design files into fully

functional and durable constructions composed of sand, metal, and glass. Once the materials in one layer have already been linked by adhesive or heat, the second layer is built, and the bonding process is repeated. It allows for the creation of formerly impossible geometries. For various automotive, commercial, and creative purposes, full-form parts are made straight from CAD data. AM is an eco-friendly production method. AM produces product samples rapidly, which is becoming increasingly beneficial since it lowers the conventional trial-and-error process, allowing newer innovations to access the market faster. It may also make customised metal things fast to replace worn or broken industrial parts.

2. APPLICATION OF AM IN THE VEHICLE INDUSTRY

Complex geometries can be costly to make using typical manufacturing procedures or extremely difficult to produce with a particular technology. Reconstruct and redesign geometries that are less expensive and lighter than origin structures can be easily created using AM technology. These approaches make it widespread in the automotive industry. It was the second most important one in the US in 2014 [8]. In 2018 SmarTech released an Additive Manufacturing in Automotive report, and *Figure 2* shows an exponentially increase in the market with an expected of $12.4 billion US in 2028. [9]

Making the lightest practical vehicle while keeping safe is a primary priority in the automotive industry which will be more friendly to the environment. Also, AM plays the leading role in many sectors like spare parts and supply chain, tooling for automotive, customisation components, and topology optimisation and Design for AM (DfAM).

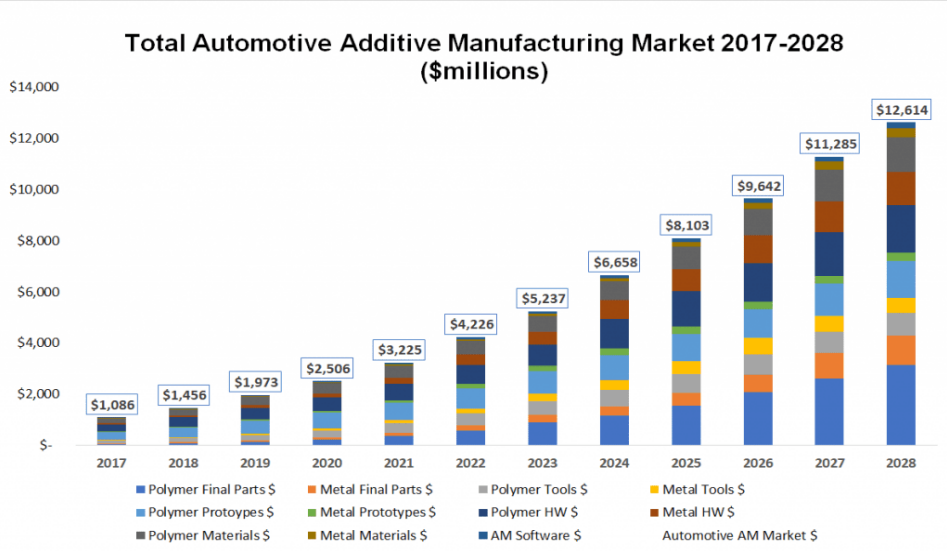

Figure 2
Total Automotive Additive Manufacturing Market 2017–2028 [9]

2.1. Growing potential of additive manufacturing on automobile components

The implementation of AM processes to develop automotive components was limited by material properties, like mechanical, thermal, and chemical behaviors under operation or surface finishing on beautifying components [10]. To increase the mechanical properties of materials, fiber reinforcements have been applied [11]. Recent advancements in carbon-fiber-reinforced filament materials have given the FDM technique a significant competitive advantage. AM equipment manufacturers have taken several methods to the length of the carbon fiber injected within the filament [12]. *Figure 3* highlights some of the existing and potential applications of additive manufacturing on automobile components [13].

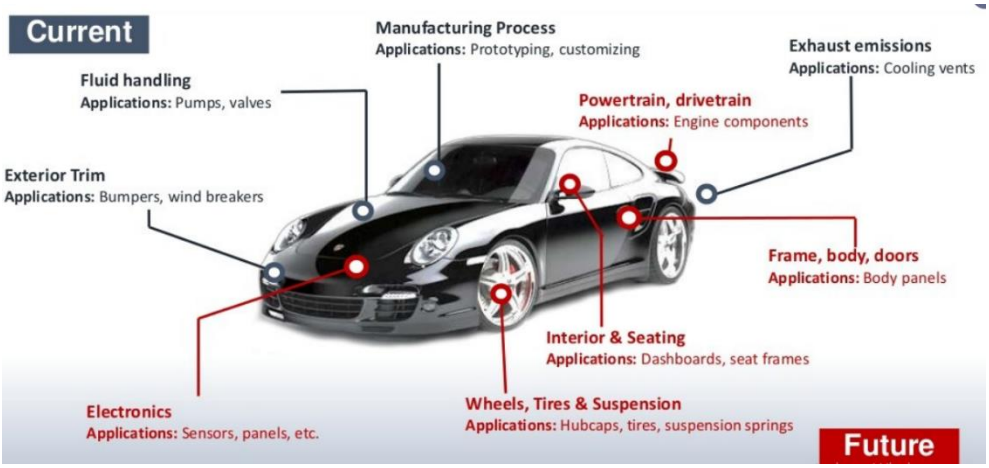

Figure 3
Some of the existing and potential applications of additive manufacturing on automobile components [13]

2.2. Effect of AM on environment

Stereolithography and laser sintering are the most common AM technologies used in the automotive industry. The key benefits of employing additive methods include weight reduction while still providing high-quality products. The reduced weight has an impact on the energy demand of a vehicle [14]. It also extends vehicles' lifecycles by allowing replacement parts to be produced faster, improves reliability, and has a modular design that allows product upgrades [15]. Electricity for machine tools, production resources (such as cutting tools), and waste all have an impact on the environment (e.g., chips, cutting fluids) [16]. Lower production weight, transportation, material losses, enhanced functionality, and the ability to print spare parts are all advantages of adopting AM technology. Potential drawbacks include increased power consumption in manufacturing and a slow printing process [17].

2.3. Stamping tooling

The demand for automobile components produced by the stamping process has risen substantially over the previous few decades, producing more than 100 million parts per year. Examples of stamped parts in the automobile sector include bumpers, chassis components, rocker rail, roof rail, and tunnels. The sheet thickness of these components can range from 1.0 to 2.5 mm [18]. AM, a technique that allows for nearly unlimited design freedom, can transform the design and manufacture of hot stamping dies. Design techniques such as topology optimisation can result in dies that employ the least amount of material while maintaining structural stability and thermal efficiency [19]. Leal et al. [18] used 3D-printed inserts in a body panel stamping tool in maraging steel DIN 1.2709, which indicated performed similarly to the traditionally manufactured inserts, but with a shorter lead time and less internal process logistics. Asnafi, N., Rajalampi, J., Aspenberg, D. et al. [17] also used AM technology in the U-bend forming tool and the results showed that AM improves the material usage and lead time significantly.

2.4. Spare parts and supply chain

As logistic operations expand in size, they get harder and harder to handle. Therefore it is crucial to assess resources to reduce risk and enhance efficiency. Distributed production of spare parts closest to the end customers may offer great benefits, including shorter supply lead – time and lower logistical costs.

According to Delic, Mia, and Daniel R. Eyers [18] and Delic, M., Eyers, D. R., & Mikulic, J. [19], AM implementatpositively influence flexible supply chain has a beneficial impact on supply chain performance. So, the AM can bring more benefits like transportation expenses are reduced. Since spare parts are manufactured at client sites or a local 3D printing supplier, there are no costs for producing tools, and spare parts production is more flexible because 3D models are easy to update. Spare-parts modifications can be made rapidly and at a low cost. They are avoiding overproduction, which occurs when more components are created and stockpiled than customers require for many reasons, and the COVID-19 pandemic is one of the most significant examples.

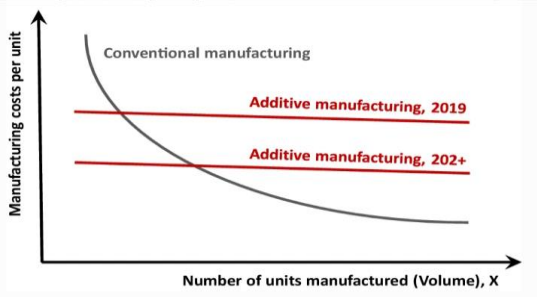

Figure 4

Conventional and additive manufacturing: manufacturing cost per unit versus the production volume [17]

As shown in *Figure 4* the conventional manufacturing is costly when the number of units manufactured decreases while AM technology shows an economical improvement in the manufacturing cost of small numbers of units manufactured.

2.5. Topology optimisation

Vehicle reduced weight is a trending topic in the automobile sector, especially among high-performance automotive manufacturers. In reality making the automobile lighter will enhance its overall stability and performance, allowing for better acceleration and greater braking. Furthermore, being less weight to transport implies better fuel economy and lower harmful emissions. Generally, every 10% decrease in car weight results in a 5-7 percent reduction in fuel usage [20]. To suggest an ideal design of vehicle parts and components, topology optimisation is implemented. AM (AM) allows for complicated designs and offers an excellent approach for fully exploiting topology optimisation. Zhu, Jihong et al. [21] illustrated the key findings and applications of the latest studies on topology optimisation and AM in the industry. *Figure 3* shows the uses of topology optimization and AM for an upright on the SAE Formula student racecar [22]. The results showed a decrease in the overall manufacturing cost by 51.7%. Another option to reduce the mass of cars the use of new materials and new manufacturing methods. [23]

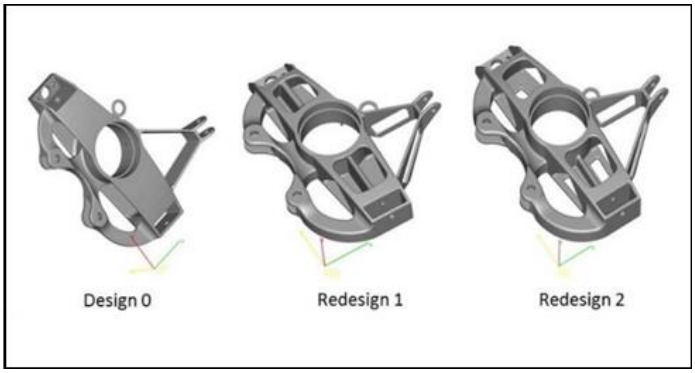

Figure 5
Using the AM and topology optimisation in-vehicle part [22]

3. SUMMARY

AM has been used to develop design iterations, improve quality through cost-effective prototyping, and make specialised tooling components [24]. Other AM pathways in automotive, however, exist that alter products and supply chains more dramatically. The main AM potentials are reducing the machining energy, which was used in high consumption rate in traditional manufacturing, transportation and logistics, and reducing waste. Furthermore, AM helps in the spare parts and supply chain

field by closing it to the end-user. It is also played a crucial role in topology optimisation with the complicity of the new redesigned parts. Optimising Stamping Die Fabrication through AM can offer a great deal of many advantages like shortening the lead time, machine shop enhancement, integration, and geometric complexity at lower costs.

REFERENCES

[1] Gordelier, T. J., Thies, P. R., Turner, L., Johanning, L. (2019). Optimising the FDM additive manufacturing process to achieve maximum tensile strength: a state-of-the-art review. *Rapid Prototyping Journal*, vol. 25, no. 6, pp. 953–971, Aug., http://doi.org/10.1108/RPJ-07-2018-0183.

[2] Vega, V. et al. (2010). The Effect of Layer Orientation on the Mechanical Properties and Microstructure of a Polymer. *Journal of Materials Engineering and Performance*, vol. 20, no. 6, pp. 978–988, Aug., http://doi.org/10.1007/S11665-010-9740-Z

[3] Vishwas, M., Basavaraj, C. K., Vinyas, M. (2018). Experimental Investigation using Taguchi Method to Optimise Process Parameters of Fused Deposition Modeling for ABS and Nylon Materials. *Materials Today: Proceedings*, vol. 5, no. 2, pp. 7106–7114, Jan., http://doi.org/10.1016/J.MATPR.2017.11.375.

[4] Rathee, S., Srivastava, M., Maheshwari, S., Siddiquee, A. N. (2017). Effect of varying spatial orientations on build time requirements for FDM process: A case study. *Defence Technology*, vol. 13, no. 2, pp. 92–100, Apr., http://doi.org/10.1016/J.DT.2016.11.006.

[5] Ahmed, F., Kilic, K. (2016). Comparison of Fuzzy Extent Analysis technique and its extensions with original Eigen Vector approach. ICEIS 2016 – *Proceedings of the 18th International Conference on Enterprise Information Systems*, vol. 2, pp. 174–179, http://doi.org/10.5220/0005868401740179.

[6] Mohanavel, V., Ashraff Ali, K. S., Ranganathan, K., Allen Jeffrey, J., Ravikumar, M. M., Rajkumar, S. (2021). The roles and applications of additive manufacturing in the aerospace and automobile sector. *Materials Today: Proceedings*, vol. 47, pp. 405–409, http://doi.org/10.1016/j.matpr.2021.04.596.

[7] Ivanova, O., Williams, C., Campbell, T. (2013). Additive manufacturing (AM) and nanotechnology: promises and challenges. *Rapid Prototyping Journal*, vol. 19, no. 5, pp. 353–364, http://doi.org/10.1108/RPJ-12-2011-0127.

[8] Wohlers, T. (2014). *Wohlers Report 2014. 3D Printing and Additive Manufcturing State of the Industry*. Wohlers Associates: Fort Collins, CO, USA, p. 226.

[9] *News on Automotive Additive Manufacturing Market Report from SmarTech*. https://www.smartechanalysis.com/news/smartec-report-automotive-additive-manufacturing-market/ (accessed Sep. 30, 2021).

[10] Singh, S. Ramakrishna, S., Singh, R. (2017). Material issues in additive manufacturing: A review. *Journal of Manufacturing Processes*, vol. 25, pp. 185–200, Jan., http://doi.org/10.1016/J.JMAPRO.2016.11.006.

[11] Zindani, D., Kumar, K. (2019). An insight into additive manufacturing of fiber reinforced polymer composite. *International Journal of Lightweight Materials and Manufacture*, vol. 2, no. 4, pp. 267–278, Dec., http://doi.org/10.1016/J.IJLMM.2019.08.004.

[12] Blok, L. G., Longana, M. L., Yu, H., Woods, B. K. S. (2018). An investigation into 3D printing of fibre reinforced thermoplastic composites. *Additive Manufacturing*, vol. 22, pp. 176–186, Aug., http://doi.org/10.1016/J.ADDMA.2018.04.039.

[13] Stefan, R. *Additive Manufacturing*. https://www.slideshare.net/StefanRadisavljevic/additive-manufacturing-43047855 (accessed Oct. 02, 2021).

[14] Hettesheimer, T., Hirzel, S., Roß, H. B. (2018). Energy savings through additive manufacturing: an analysis of selective laser sintering for automotive and aircraft components. *Energy Efficiency*, vol. 11, no. 5, pp. 1227–1245, Mar., http://doi.org/10.1007/S12053-018-9620-1.

[15] Javaid, M., Haleem, A., Singh, R. P., Suman, R., Rab, S. (2021). Role of additive manufacturing applications towards environmental sustainability. *Advanced Industrial and Engineering Polymer Research*, Aug., http://doi.org/10.1016/J.AIEPR.2021.07.005.

[16] Burkhart, M., Aurich, J. C. (2015). Framework to predict the environmental impact of additive manufacturing in the life cycle of a commercial vehicle. *Procedia CIRP*, vol. 29, pp. 408–413, http://doi.org/10.1016/J.PROCIR.2015.02.194.

[17] Böckin, D., Tillman, A. M. (2019). Environmental assessment of additive manufacturing in the automotive industry. *Journal of Cleaner Production*, vol. 226, pp. 977–987, Jul., http://doi.org/10.1016/J.JCLEPRO.2019.04.086.

[18] Leal, R. et al. (2017). Additive manufacturing tooling for the automotive industry. *The International Journal of Advanced Manufacturing Technology*, vol. 92, no. 5, pp. 1671–1676, Mar., http://doi.org/10.1007/S00170-017-0239-8.

[19] Chantzis, D. et al. (2020). Review on additive manufacturing of tooling for hot stamping. *The International Journal of Advanced Manufacturing Technology*, vol. 109, no. 1, pp. 87–107, Jun., http://doi.org/10.1007/S00170-020-05622-1.

[20] Asnafi, N., Rajalampi, J., Aspenberg, D., Alveflo, A. (2020). Production Tools Made by Additive Manufacturing Through Laser-based Powder Bed Fusion. *BHM Berg- und Hüttenmännische Monatshefte*, vol. 165, no. 3, pp. 125–136, March, http://doi.org/10.1007/S00501-020-00961-8.

[21] Delic, M., Eyers, D. R. (2020). The effect of additive manufacturing adoption on supply chain flexibility and performance: An empirical analysis from the automotive industry. *International Journal of Production Economics*, vol. 228, p. 107689, Oct., http://doi.org/10.1016/J.IJPE.2020.107689.

[22] Delic, M., Eyers, D. R., Mikulic, J. (2019). Additive manufacturing: empirical evidence for supply chain integration and performance from the automotive industry. *Supply Chain Management: An International Journal*, vol. 24, no. 5, pp. 604–621, Aug., http://doi.org/10.1108/SCM-12-2017-0406.

[23] Garai, F., Béres, G., Weltsch, Z. (2020). Development of tubes filled with aluminium foams for lightweight vehicle manufacturing. *Materials Science and Engineering: A*, vol. 790, 139743, ISSN 0921-5093, https://doi.org/10.1016/j.msea.2020.139743

[24] Fedorko, G., Molnar, V., Dovica, M., Toth, T., Kopas, M. (2014). Analysis of pipe conveyor belt damaged by thermal wear. *Engineering Failure Analysis*, 45, pp. 41–48.

Design of Machines and Structures, Vol. 11, No. 2 (2021), pp. 14–20.
https://doi.org/10.32972/dms.2021.010

DEVELOPMENT AND MANUFACTURING OF AN EXPERIMENTAL FLAT WHEEL STRAIN WAVE GEAR UNIT AT K.K.K. 99 LTD

BALÁZS GÖNCFALVI – GÁBOR OFFRA – RÓBERT KRISCH

K.K.K. 99 Kft., info@kkk99.hu

Abstract: The functions of the main components of a flat-wheel harmonic drive are similar to the functions of a traditional harmonic drive, but the features of the flexible and the solid wheels are different. This paper reports the development and investigation of the experimental flat wheel harmonic drives. The development project was sponsored by Ministry for National Economy.

Keywords: *development and investigation, harmonic drive, Ministry for National Economy*

1. INTRODUCTION

The K.K.K. 99 Kft. has received a grant in the GINOP 2.1.7-15 tender for research and development of flat wheel strain wave gear drives. The design of the teeth, the ideal shape of deformation and the other functional parts highly influence the behavior of the device and also the manufacturing cost. This article deals with the development of all the different combination of potential drive units as well as their tests and their evaluation. Our goal was to develop a flat wheel strain wave gear unit, which can be a competitor for the currently available cylindrical alternative.

2. THE WORK PRINCIPAL OF FLAT WHEEL STRAIN WAVE GEAR DRIVE

The mentioned flat wheel strain wave gear is a special variant of the generally known harmonic drive. It consists of a rotational wave generating input element with a cam surface on its axial extent (4), a flexible axial bearing (3), which indirectly also deforms a flexible wave gear element (2), thus connecting it to the rigid gear (1) and in return, turning it. These are the main parts of the gear unit, which is illustrated in *Figure 1*.

A double wave gear unit connects on two opposite edges which means that one turn of the input element only turns the flexible gear for two teeth divisions. This all implies that this design can achieve a very high gear ratio (i = 80 – 320). [2]

For the desired movement it is required to guarantee the ideal teeth parameters (deformation, teeth shape, teeth gap, etc.) for the connection of the two main gear elements without teeth head overlap or teeth head interference. The teeth surface geometry is determined by a deformation and teeth connection model reported in a previous study [2], while the flexible wave gear deformed shape was calculated by using finite element method.

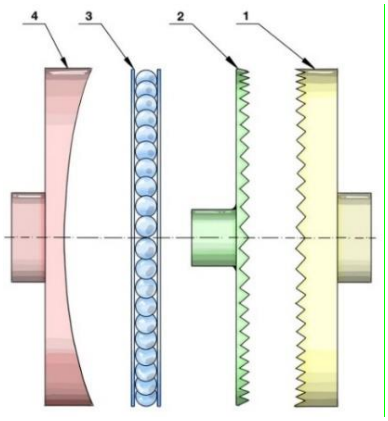

Figure 1
The main elements of a flat wheel strain wave gear unit: rigid gear (1), wave gear (2), flexible bearing (3), wave generator input cam (4)

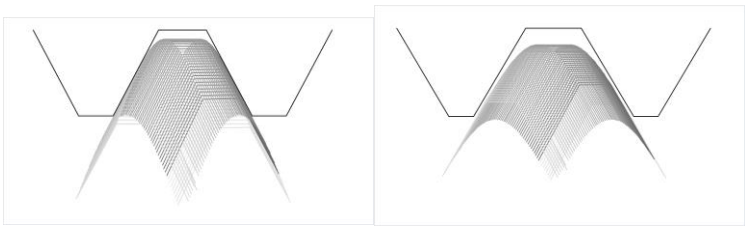

Figure 2
The plot of one teeth of the flexible gear in the rigid counterpart in unloaded condition on the outside (left) and on the inside (right) edge

3. DESCRIPTION OF THE DEVELOPMENT PHASES

For the validation of the analytic and finite element calculations, real word tests must be carried out hence the goal of the project was to produce prototypes. Prior to the examination the design phase took place where the manufacturing, assembly and other cost driving aspects were considered resulting in the best combination of geometry. Next, all the considered parts were manufactured with different movement influencing versions so that we were able to assemble seven distinct drive units for comparative tests. Based on the results we were able to determine the effect certain parts have on the behavior of the drive unit and to understand the advantages or disadvantages of the developed devices. These results will greatly influence the position of the product on the market and its place in the industry.

Figure 3
Exploded view of the designed flat wheel strain wave gear unit

4. CONCEPTIONAL DESIGN, THE CHOSEN DRIVE COMBINATIONS

During the research other types of precision drives were evaluated. Based on these results we had many different mechanical options and combinations which can cost-effectively fulfil the requirements. We also had the possibility to choose from many kinds of materials, lubricants and fasteners.

The first step was to achieve the proper bearing arrangement of the four main elements illustrated in *Figure 1*. Next, the special torque motor's stator and rotor were installed. Since it is very compact its installation must meet certain requirements from the manufacturer. The connection of all these is the drive housing which has adjustments for assembly and connecting surfaces for electrical components. It is important to mention the special four wire bearing maintaining the vital output stiffens.

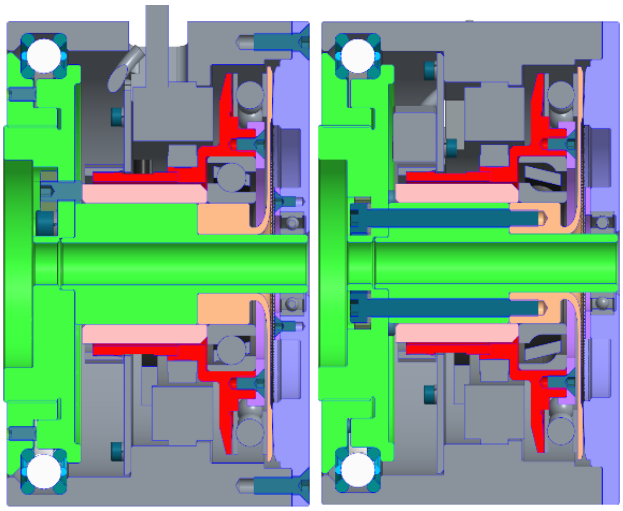

Figure 4
Section of the final strain wave gear unit design

The main elements were manufactured in different variants so that we can have a ratio of 120 or 160, different cam surfaces and various flexible bearing sizes. We also had multiple sensor options and drive houses with or without heat sink grooves.

5. TEST ARRANGEMENTS AND USED MEASURING INSTRUMENTS

For standardizing the tests we have created a robust stand, shown in *Figure 5*, which can hold all the different gear unit combinations. The unit installed on this mount can be loaded with a steel brake rotor and copper brake pads or for low displacement with a steel bar and weights.

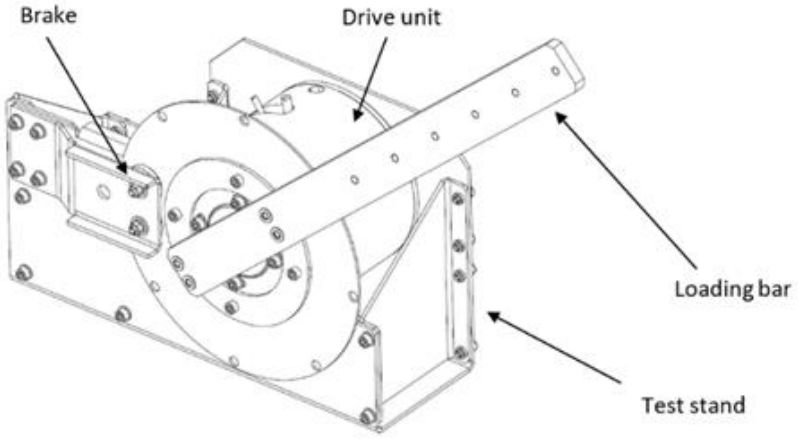

Figure 5
Test stand for prototype gear unit tests

On the outer edge of the loading bar we can measure the displacement with an indicator dial gauge. For torsional stiffness measurements we first had to determine the displacement of the test environment. For this we replaced the drive unit with an equally sized but prominently stiffer component, which was loaded the same way as the gears would be. Since we worked out the displacement of the other elements (table, loading bar, adapters, test stand) we can deduct the real torsional stiffens of only the gear unit itself. During the tests we recorded the required electrical current and also the deflection, which gives us the overall angular stiffness.

With the same arrangement we can also measure position repeatability, which is crucial for precision drives. For this we had a constant torque load moving from horizontal position to a –30[°] and then back again to see how much error accrue.
The application of these drives in some of the areas requires long lifetime. To simulate these conditions, we measured the drawn current, the temperature of the housing and the motor and the noise level while increasing the load and the speed. The temperature gain was measured with the resistance probe of a multimeter while the distribution was inspected with a thermal imaging camera. We used a sound level meter to determine the noise level. While these measurements were adequate to compare

different constructions the data was heavily influenced by the surrounding environment's amplifying effect.

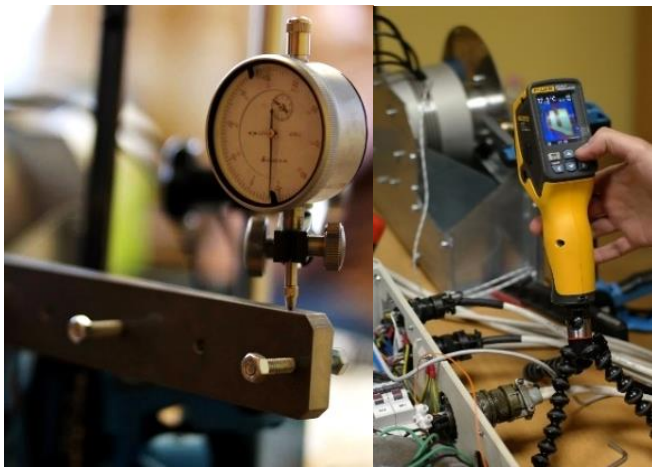

Figure 6
Displacement and position repeatability test with an indicator dial gauge, heat distribution inspection with a thermal imaging camera

6. TEST RESULTS

During the tests we examined seven different drive combinations. The different combinations were created by choosing the appropriate options from the configuration table shown below.

Table 1
Drive unit configuration table

Generator input unit	2° ball bearing	2.3° ball bearing	2 roller bearing
Bearing size	1.25 - 0.4 mm	1.4 - 0.5 mm	
Encoder	Inc. D20	Inc. D80	Analog
Gear ratio	120	160	
Housing	Smooth	Grooved	

To record the test results, we created a standardized report sheet. This document contains all the used parts and the results of all the test, including the position repeatability, torsional stiffens and the lifetime simulation. During the measurements we had the possibility to observe the different electrical parameters in real time for the motor controller. These were the drawn current, voltage, speed, position target and difference. For example, we were able to detect that at higher speeds stronger controller manipulation was needed due to the slight runout of the angular contact bearing.

With these tests we have gained a great amount of experience. The analog encoder sensor had shown that while it was able to work with the drive system it lost signal at higher speeds and temperatures. This meant we could only achieve significant

results with a digital transmitter. While the gear set with a ratio of 160 required more current it was also a bit less noisy at higher speeds. On the thermal images it was clearly shown that the housing with grooves provided a lot better cooling for the motor.

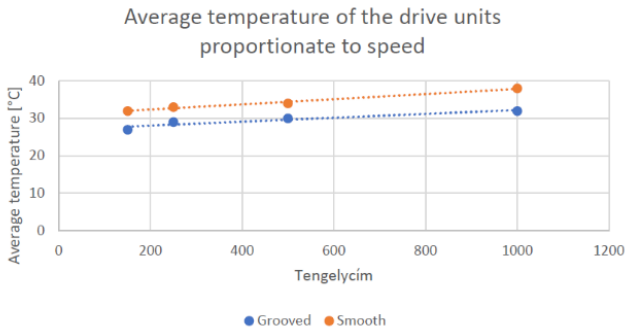

Figure 7
Temperature gain difference between grooved and smooth housing

The position repeatability test showed that the higher resolution D80 encoder does not have much advantage against the D20 variant since with the same gear set the rotational error was repeatedly lower than an arcminute. The installation of the axial-angular contact roller bearing resulted in a lower noise level opposed to the ball bearing variant, but it also meant a higher runout and a higher current consumption.

7. ITS PLACE ON THE MARKET

It can be admitted that for a commercially available drive the ratio of 120 or 160 is quite high, in this field mostly planetary gears are on the market. We can further narrow down the competitor products since ours is a compact system joined with a servo drive so it can work independently while its size is also moderate at Ø 133 × 100 [mm]. The average position repeatability is 0.7 [arcminute] which is also an impressive value. Mean torsional stiffness being just above 6.2 [Nm/arcminute] is comparable to that of the Bonfiglioli precision planetary drives' with similar power capabilities.

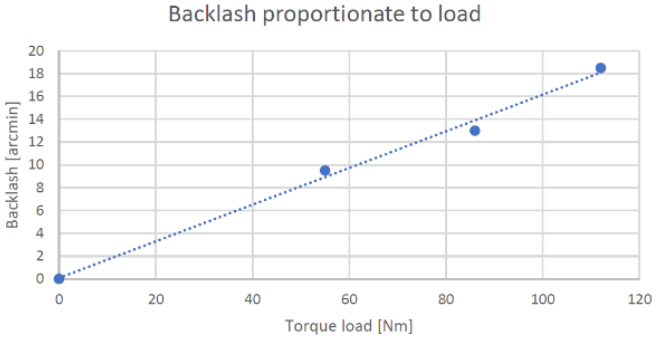

Figure 8
Backlash in regards to torque load

One of the main advantages of the developed drives is that we are able to set up the teeth connection with stepless dial. Its effect is shown in *Figure 8* where we can see that the backlash stays below 2 [arcminute] until 10 [Nm] torque load, which is above the capabilities of the Bonfiglioli drives that have 4-6 [arcminute] of backlash.

8. FURTHER DEVELOPMENT POSSIBILITIES

The research of the strain wave drives resulted in a lot of new experience, which can influence a more advanced generation of prototypes. Our next goal is to implement such modifications that can further optimize the device parameters. The flexible axial bearing could be used with smaller ball bearings to improve running properties. Or using oil lubrication on the teeth could lower resistance. In this case we need to provide the sealing for the whole unit but this would mean lower frictional losses, lower noise level and would also benefit the heat dissipation. All the examined drive units are the same size but they can be configured in a way to suit the different use cases.

This research was supported by the European Union and the State of Hungary in the framework of GINOP-2.1.7-15-2016-00507.

REFERENCES

[1] www.harmonic-drive.com.

[2] Krisch R. (2010). *Síkkerekes hullámhajtó-művek fejlesztése*. PhD study, BME.

[3] Kardos Sz., Krisch R. (2018). Síkkerekes hullámhajtómű fejlesztése a K.K.K. 99 Kft-nél. *GÉP*, LXIX. évf., 4 sz., p. 41.

[4] www.bonfiglioli.com.

Design of Machines and Structures, Vol. 11, No. 2 (2021), pp. 21–27.
https://doi.org/10.32972/dms.2021.011

DEVELOPMENT OF A PRECISION DRIVE UNIT AT K.K.K. 99 LTD TO BE UNIVERSALLY USED AS ROBOT JOINTS WITH HIGH POWERDENSITY AND MODULAR CONSTRUCTION

RÓBERT NEUMANN – GÁBOR OFFRA – RÓBERT KRISCH

K.K.K. 99 Kft., info@kkk99.hu

Abstract: A highly innovative gear unit set has been developed and manufactured to be widely used in medical industry, manufacturing robots or high precision manipulators. The main elements of the drive unit are the gear ratio reducing strain wave gear, the torque-motor and the force-torque measuring sensor, which can be combined arbitrarily. In one unit the motor series size is given but its power output (longer motor) and the gear reduction ratio can be varied. Assembling these parts, the result of this RnD project is a high precision drive with minimal dimensions, which, on itself, is able to position rotating movement precisely and while at halt it can also keep that position with high torsional stiffness. What makes the modular precision drive unit whole, is the controlling system. The above-mentioned machine elements can be assembled into different configurations so it can become part of a SCARA, humanoid or Delta robot. As a result of this project the created precision drive prototypes could provide tests and results that may influence the mechatronic and mechanical engineering profession.

Keywords: *research and development, high precision, strain wave gear*

1. INTRODUCTION

The K.K.K. 99 Kft. has received a grant in the 2018-1.1.1-MKI-2018-00152 tender to develop and manufacture a high precision drive system that can be widely used as rotational joints in medical and industrial robots or high accuracy manipulators. The present paper deals with the construction of these drives, their properties, the tests they undergone and their results. After describing the different types of precision drives we evaluate the outcome.

2. THE WORK PRINCIPAL OF THE STRAIN WAVE DRIVES

Strain wave drives are high ratio, backlashless, high power density precision drives. *Figure 1* illustrates their main elements. It consists of a rotational wave generating input element with a cam surface on its axial extent (3), a flexible axial bearing (3) which indirectly also deforms a flexible wave gear element (2) thus connecting it to the rigid gear (1) and in return turning it. The latter two elements both have a trapezoid tooth shape, the difference is that on the flexible wave gear there are fewer teeth by the amount of cam tips the generator has. These parts are all coaxially positioned

so the unwanted imbalance effect of cycloidal drives is not present here to restrict the top speed of the input.

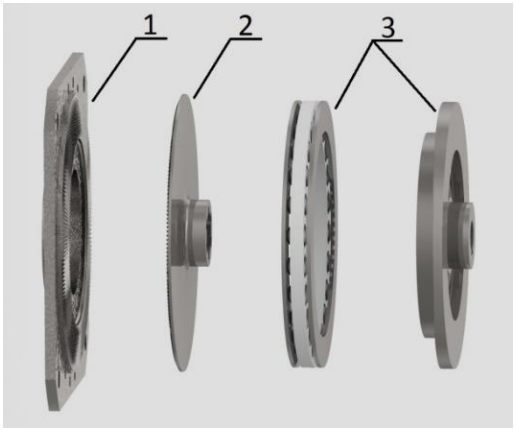

Figure 1
The main elements of the flat wheel strain wave gear unit: rigid gear (1), wave gear (2), flexible bearing and wave generator input cam (3) [3]

There are different designs of strain wave gears. The industry uses mostly the cylindrical type, which teeth are on the cylinder mantle of the elements. However, there is also a flat wheel type that has the teeth on the front of a round disc and the deformation is in the axial direction rather than the radial.

Figure 2
Experimental cylindrical and flat wheel strain wave drives

During this tender project the four strain wave gear unit shown in *Figure 2* were manufactured. Two flat wheel and two cylindrical strain wheel version was built, which can both be with and without an integrated brake. Some parts in these drive units are interchangeable so it was possible to try out different combinations. As a result of this the input generator's cam profile and the rolling elements of the flexible bearing can be varied during the tests.

3. INTRODUCTION OF THE TEST ENVIRONMENT AND THE INSTRUMENTS

In order to examine our drive units, we had to construct a specific test environment and choose the adequate measurement instruments. These will help us collect the data we need to compare the properties of each configuration to one another and also to the competitors on the market. We can categorize the tests into two groups. First, the test stand shown in *Figure 3* was constructed to measure the base parameters of each drive. This structure is made from steel plates and bars to have a solid foundation, here we can load the gear units with a steel brake rotor. It is also equipped with a force measuring device that makes it possible to monitor the given load in real time. This force sensor is connected to a signal amplifier then the data is filtered by the software. This data is forwarded to a PC by a National Instruments USB-6212 multifunctional data acquisition device. Further measurements were made with a FLUKE Ti110 thermal imaging camera and an Agilent U1732 LCR meter. An LCR meter is a type of electronic test equipment used to measure the main physical parameters (inductance, capacitance, and resistance) of an electronic component.

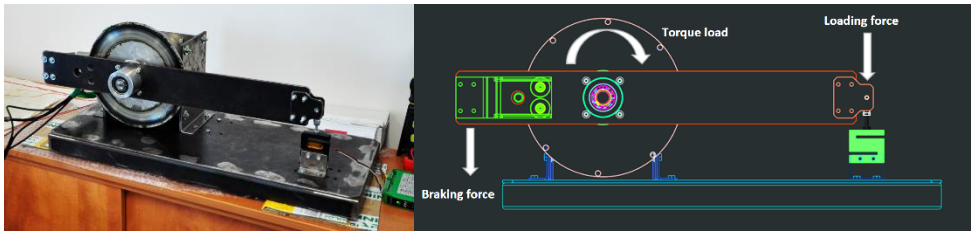

Figure 3
Test stand for the drive units

Several important results came from these tests. We got to measure the drawn current for several load sets, the temperature gain in each state on the housing and on the brake, the frictional losses and the position repeatability for the gear sets. Next, we constructed a manipulator that had flat wheel strain wave drive as its first joint and cylindrical wheel drive as the second and third.

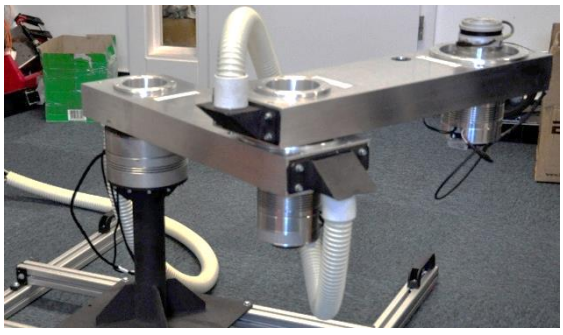

Figure 4
Manipulator with strain wave drives

This assembly mostly resembles a SCARA robot and specialized for testing the developed precision drives as they would be used and equipped in robots, which would be their most common field of use. With this manipulator we were able to conduct further tests. The vertical deflection, the rigidity of the system all together and the position repeatability was measured with this structure.

4. RESULTS FROM THE FLAT WHEEL (SV2) STRAIN WAVE DRIVE

We began with the measurement of drawn current at different load and speed levels for the flat wheel drive. The results ranged from 2.5–7.5 [A] depending on the load. It is clearly shown in *Figure 5* that the current for the motor is increasing with the load and the speed but with decreasing increments.

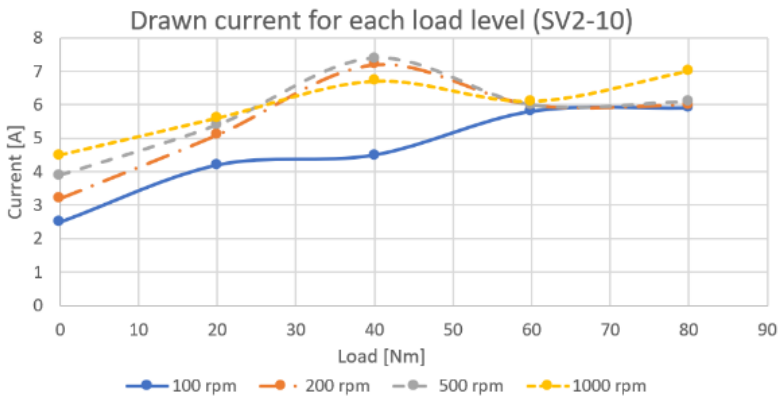

Figure 5
SV2-10 drive unit current drawn

At the peak of the control unit's power, which is 10 [A] at 500 [RPM], the drive unit equipped with a brake was able to produce 183 [Nm] torque while the brakeless version 175 [Nm]. These results are quite impressive for a drive with these dimensions. Only the flat wheel units have an integrated temperature sensor so that measurement was only possible with these. As expected, both the internal sensor and the thermal camera showed temperature gain proportional to the time.

Last, we measured the torsional stiffness and position repeatability. For the position repeatability test we mounted a laser pointer to the end of the arm then moved back and forth the drive (60°–90°) and observed the error that accrued at the distance of 10.5 [m]. According to the visual observation the start and end point difference resulted in 0.0055° for the position repeatability. To ensure good measurement we also evaluated the data from an encoder on the output shaft, which gave 0.0035° error for the drive unit with brake and 0.0036° for the brakeless version. For torsional stiffness we calculated 0.07 [arcminute/Nm] at 35 [Nm] torque load for the SV2-10 drive. This is a decent advantage compared to the currently available precision drives.

5. TEST RESULT WITH THE CYLINDRICAL STRAIN WAVE DRIVE (HHH)

The main advantage of the cylindrical type drive is that the flexible elements are far easier to deform thus presenting less force on all of the moving parts. This also means less current drawn for the motor during operation 0.3–4.5 [A] and better mechanical efficiency.

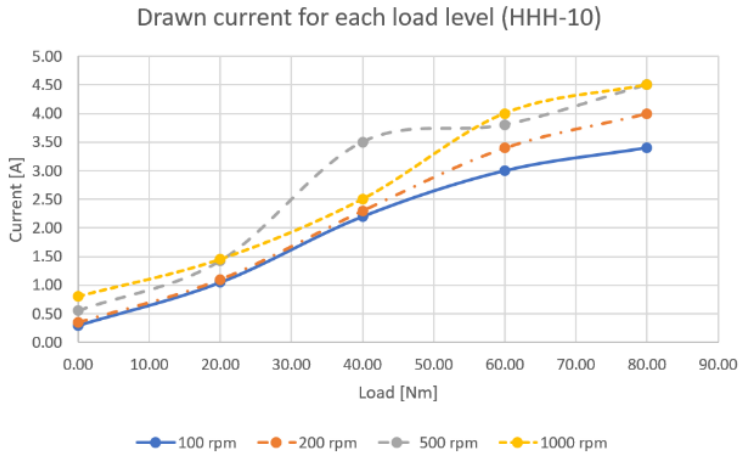

Figure 6
Current drawn by the HHH-10 drive system

Less frictional loss results in less temperature gain, so the temperature stayed below 27 [C°] after the initial fluctuation. The manual position recovery test shows similar results with the flat wheel drives but using the digital encoder we recorded 0.0044° error, which means these are a couple thousandths less accurate than the competition.

6. TESTS WITH THE ROBOT CONFIGURATION

We carried out three important tests with the experimental manipulator. For real time force and torque measurements we mounted an OnRobot HEX-H sensor on the end of the last arm, which allowed us to measure the effect different loads have on the whole assembly in real time.

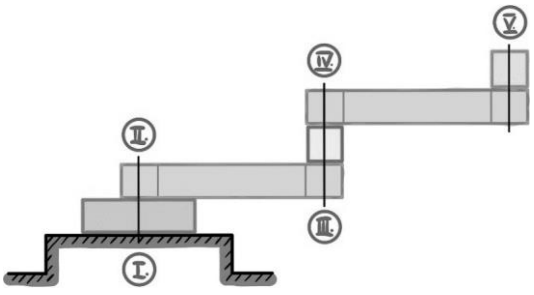

Figure 7
Experimental robot configuration with designations for each highlighted point

We measured the vertical deflection at the highlighted points shown in *Figure 7*. The results revealed that on the first joint, which is constructed with a flat wheel drive, significantly less deformation occurred than on the other two with their cylindrical drives. We also calculated the torsional stiffness of each joint and the whole system while maintaining a uniform sideways load on the structure. The six-axis sensor was used to accurately measure the given load, then these values were combined to obtain the overall stiffness from the displacement.

Finally, we measured the position recovery error after a complicated series of movements back and forth, then back to the starting position. For this we defined a course for the robot to follow a couple of cycles and then observed the same laser pointer start and end position like we did at the torsional stiffness and vertical deflection tests.

7. COMPARISON AND SUMMARY OF RESULTS

After all the tests, the results were summarized and compared. It is important to mention that for all four torque motors the parameters measured with the LCR meter were slightly different from the catalog values so we applied the recorded amount. The flat wheel strain wave drives are less sensitive since they needed relatively less power as we increased the load, although they needed more at just idle states, which means they are less efficient to run at low conditions. They also have a better torsion stiffness and their position recovery error is just 0.0035°, which makes them more robust than the cylindrical types.

The cylindrical strain wave drives needed less torque to idle but their power consumption increased rapidly with the given load. This concludes that it is better to use it at lower loads. Their torsional stiffness is a bit modest compared to the flat wheel types, it is most likely due to the geometry of the flexible elements, which allow for more displacement at less torque. Since their position repeatability is 0.0044° they are less accurate than the competition.

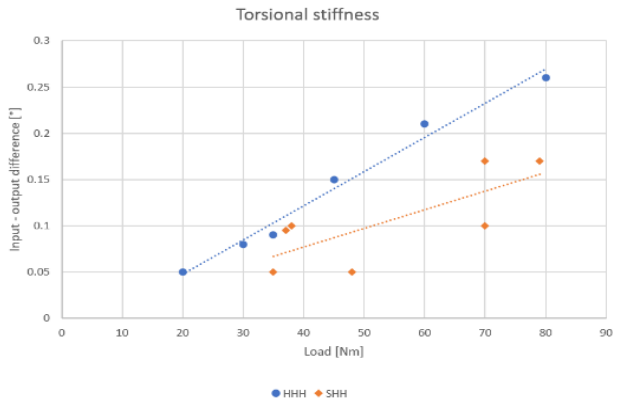

Figure 8

Rotational deflection increase with the gained load for both the flat and cylindrical strain wave gear set

In *Figure 8* you can see how the rotational deflection increased as the load gained for both drive types. It is necessary to mention that these results for both units are far better then what the currently available industrial precision drives can offer.

The tests carried out with the manipulator proved that the robot arms deflected less than the drives, since their complicated construction allowed more elasticity but the overall displacement is still very low. Torsional stiffness measurements showed similar results. The most significant result is the position recovery error of the whole system since it is only 0.05° after two cycles.

8. SUMMARY

After concluding the tests and measurements, it is clear that the precision drive system developed by the K.K.K. 99 Kft. has achieved the expected results, which makes them suitable for the required tasks. Our future plan is to utilize the accumulated experiences and knowledge to further dial in the existing drive units and also to develop a line of products from them.

This research was supported by the Ministry of Innovation and Technology in the framework of 2018-1.1.1-MKI-2018-00152.

REFERENCES

[1] www.harmonic-drive.com.

[2] Krisch R. (2010). *Síkkerekes hullámhajtó-művek fejlesztése*. PhD study, BME.

[3] Kardos Sz., Krisch R. (2015). Síkkerekes hullámhajtómű alapelemeinek optimálása. *GÉP*, 6. sz., pp. 65–68.

Design of Machines and Structures, Vol. 11, No. 2 (2021), pp. 28–35.
https://doi.org/10.32972/dms.2021.012
http://orcid.org/0000-0002-0329-2905 (B. Kriston)
http://orcid.org/0000-0003-0749-7569 (K. Jálics)

BENEFITS AND LIMITATIONS OF ACOUSTIC METHODS IN THE VEHICLE TRANSMISSION DIAGNOSTICS – A CASE STUDY

JÓZSEF BALÁZS KRISTON – KÁROLY JÁLICS

University of Miskolc, Department of Machine and Product Design
3515, Miskolc-Egyetemváros
machkbj@uni-miskolc.hu

Abstract: In general, for the diagnostics of a faulty machine several diagnostic methods can be considered. In this paper, the benefits and limitations of the acoustic diagnostic methods are shown, based on a noise problem of a real car with a 6-speed manual transmission. The possible diagnostic methods will be pointed out, and an analysis will be performed with noise and vibration measurements on the car. Based on the analysis conclusions regarding the benefits and limits of the used diagnostic method will be drawn.

Keywords: *transmission, diagnostics, noise, vibration*

1. INTRODUCTION

The sale of passenger vehicles word wide is steadily increasing nowadays. Every car containing a powertrain, incl. a gearbox (also electric cars can have a gearbox), which is one of the most important and expensive components of the car. Its repair in case of a failure can be very expensive, regardless of the type of the gearbox. Nevertheless, the repair costs of automatic gearboxes (planetary, DCT, CVT) can explode. In case of an older vehicle a necessary repair could even mean a financial total loss. The detection of a failure in the gearbox in early phase could also mean cost saving.

The only problem for this intention is that a diagnostic method must be applied, which is able to indicate the failure's characteristics and location. The method should be simple to use and low budget. Next chapter shows some of the most promising methods for that purpose.

2. POSSIBLE DIAGNOSTICS METHODS

Practically, the vehicle diagnostics is the whole bulk of measurements and evaluations performed with diagnostics methods for vehicle condition inspection. This kind of monitoring process can be accomplished for various reasons, e.g., maintenance, repair, official technical inspection, service–operation, detection of defects, failure prevention, end-of-line test, assessment of operational safety or vehicle value, judicial technical investigation etc. In engineering practice, the diagnostics is performed through

the observation of physical parameters such as temperature, rotation speed, pressure, flowrate, pressing force, torque, impedance, magnetic flux, noise/vibration values etc. that characterize the condition of engineering systems. In case of offboard diagnostics the required hardware and software do not integrated in the vehicle's mechatronic system, while the onboard diagnostics is the own function of the vehicle.

One of the tasks of motor vehicle diagnostics is to determine the wear and tear of system components i.e., which lifetime stage they are. Mechanical systems usually contain several frictional surfaces. For example, the piston-cylinder-piston ring assembly group, the valve control-system and bearings of internal combustion engines (ICE). Due to the friction the clearances between the elements are increasing, which can lead to troubles: excessive oil consumption, combustion problems, hard idle, decreased power, strange noises, leakage, etc. *Figure 1.* shows the lifetime diagram of before – mentioned assembly group in function of amount of escaped crankcase gas, but the oil consumption or compression pressure could be the indicator of the same issue.

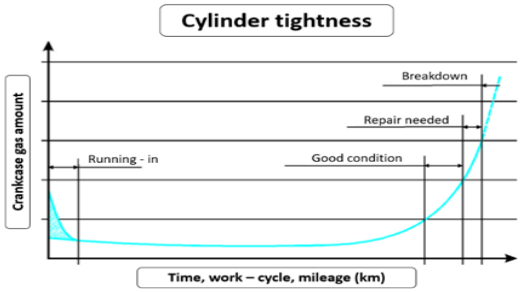

Figure 1

Characteristic diagram of machine elements due to wear [1]

Because of growing abrasion, the function loss is worsening at first in a small compass and then exponentially, as in case of tire tread. The function loss results from wearing affects disadvantageously other parts as well, e.g., the wrecking of damper's damping ability influences the function of ABS and ESP systems negatively. Apart from cylinder tightness measurement wide range of offboard diagnostic procedures are existing for ICEs; not exhaustive list: torque and mechanical power loss measurement on test bench; emission/temperature/exhaust noise/compression pressure/ battery voltage measurement on brake pad; etc. [1].

In our days modern cars are mounted up with lot of electrical devices and sensors to stabilize driving and monitor the behaviour of vehicle units. Onboard diagnostics (OBD) invented for continuous or periodical self-diagnose of degrading components and vehicle's emission system. When a problem occurs the malfunction indicator lamp (MIL) flashes on dashboard and the system stores a diagnostic trouble code (DTC) in engine control unit (ECU). A diagnostic scan tool (Generic Scan Tool) or code reader can communicate with microprocessor that allows for the service technician to retrieve information regarding the fault. As cars become more complex, it is required to extend the functionality of OBD over remaining

parts of vehicle and not only emission control system. Recently, the data result from OBD system used not exclusively in maintenance services but utilized in vehicle development as well [2].

The vibration signal is sensitive to all faults, while other measurements – mentioned above – able to detect only some specific faults. It is well known that due to the malfunctions and wearing of machine elements during operation the emitted noise and vibration values change compared to the intended operating conditions. Therefore, the noise and vibration analysis technically can be an efficient tool for faulty condition detection. In this cited work [3], fault diagnostics of gear transmission system via vibration signal analysis is performed. In order to examine the vibration condition of a gearbox a test rig was created. With the help of time and frequency domain analysis gear defect was revealed and categorized successfully. Puchalsk [4] presented a diagnostics method of valve system of a spark ignition (SI) engine based on vibration acceleration signals. The technique based on mathematical processes, namely the lower triangular orthogonal (LQ) factorization and the singular value decomposition (SVD). The method uses vibration time series data after angular resampling without transformation in the frequency domain. With this method the status changes of valves are investigated. The method was verified by experimental tests of the engine valve systems. An automated diagnostics system [5] was established based on Artificial Neural Network (ANN) to determine various malfunctions in internal combustion (IC) engines such as misfiring, piston slap and bearing knock. It was exhibited that the network fed with simulated data can properly reveal the location and severity of faults. Regarding mechanical failures the data for the network training came from envelope analysis of vibration signals and in case of combustion faults it came from torsional vibration of crankshaft and angular acceleration of engine block.

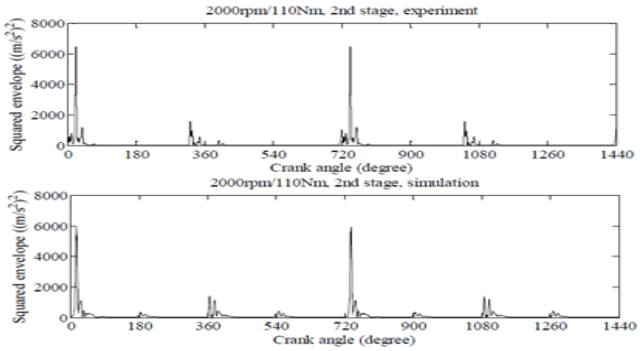

Figure 2

Simulated and experimental envelope signals with 2nd stage piston slap fault [5]

Currently, number of techniques are available for engineers to predict malfunctions and specify the reason of failures. With the appears of control systems the diagnostics transferred from outside to inside the vehicle and became continuous. Moreover, diagnostics procedures based upon vibration and noise analysis increasingly utilized in engineering practice.

3. PROBLEM DESCRIPTION AND TESTS

A relatively new passenger car (year of manufacture: 2019) is given with a turbo charged direct injection 1.5 Litre petrol engine, front wheel drive with a 6-speed manual transmission. After about 6 months of using the car, the owner complaining about a certain noise during gear shift up from gear 1 to gear 2, resp. from gear 2 to gear 3. We assume, that the noise is also existent at the other gear shifts (3-4, 4-5, and 5-6), but in these cases due to the higher speed the rolling noise masks the failure noise originated from the gearbox.

The characteristics of the noise can be described as impact or hit noise; in terms of frequency content, it can be characterized subjectively as a sharp noise. The noise can be clearly heard inside and outside of the car during shifting and it is very disturbing for certain persons sitting in the car. The analysis is problematic, since some of the passengers may not find the noise to be very disturbing, some of them do not even notice it. Nevertheless, the problem was immediately reported to the dealer after discovering, who replaced several components, e.g., the clutch, the axle-shafts, and the gearbox one after the other. This repair tries failed; the noise still can be a heard. The dealer refuses any further repairs or other measures, he claims the car is ok. despite of the still existing noise.

Our task is therefore to analyse the problem without disassembling the gearbox, in order not to lose the guarantee. First a pass-by noise measurement was performed in order to identify the noise characteristic, and to make sure the noise is really existent. For outer noise measurement of a passenger car there is a standardized measurement (ISO 362: Measurement of noise emitted by accelerating road vehicles — Engineering method — Part 1: M and N categories). In our case due to the characteristic of the noise it was not constructive to perform the standardized measurement, since this has to be performed during the accelerated ride in a certain gear speed (e.g., in 2. or 3.). However, the disturbing noise is generated only by gears shifts. Thus, we used an approx. 30 m long light slopy road with one lane and the car was started from the stillstand in gear speed 1 and was driven uphill. After a few meters of driving the gear speed 2 was shifted through the driver. At the start of the car until the stop the raw time signal of the sound pressure was recorded *(Figure 3)*. The microphone was positioned 4 m from the middle of the road. The overall measurement length was 10 s from start to stop of vehicle. The measurement was performed with a single channel analyser. The measurement was repeated several times, and the noise phenomena could be reproduced in every tests.

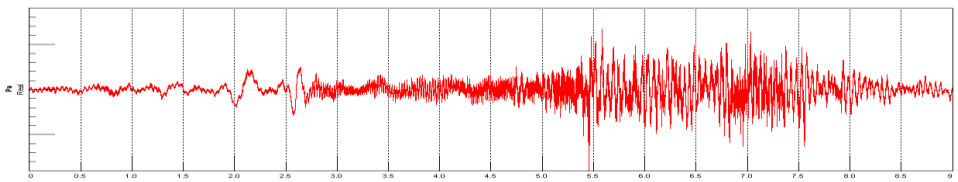

Figure 3

Pass-by noise time signal

In order to get closer to the failure a static state measurement of the car was also performed. In our case we put the car on the lifting platform, and we disassembled the lower engine protection panel. In that way the engine-gearbox unit could easily reached and could be moved back and forth by hand against the pendulum support. At this rhythmic movement of the unit a sharp impact/hit noise could be heard, as something might be loose in the gearbox, and this part is hitting another one. The noise was very similar to that which was recorded at the pass-by noise measurement. Subjectively the source of the noise could be in the gearbox. For the more exact localization a near field microphone was applied close to the gearbox surface. In addition, accelerometers were mounted to the gearbox housing in order to measure the vibration *(Figure 4)*.

Figure 4

Accelerometer locations (red circles) on the gearbox housing (left: point 1; right: point 2)

The raw time signals of sound pressure and vibrational acceleration were measured approx. 8 s long, with the sampling frequency of 48 kHz with a single channel analyser, thus the noise and the acceleration in the 3 measurement positions were recorded sequentially. The raw time signals can be seen in *Figure 5*.

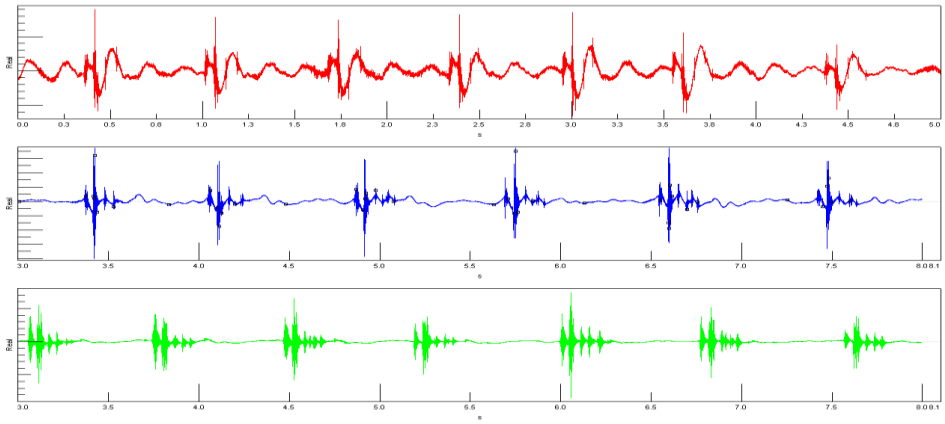

Figure 5

Time signals at the standstill measurements (top: sound pressure; middle: acceleration point 1; bottom: acceleration point 2)

4. THE ANALYSIS

Based on the raw time signals from the pass-by and standstill measurements, in the post processing of the time signal the spectrograms and averaged spectrums were created by the Fast Fourier Transformation. The goal was to find frequency contents, which may refer to a failure of a certain component of the gearbox.

Figure 6 shows the frequency content of the time signal of the pass-by noise. The frequency range of the noise approx. 4000 Hz wide and there are only a few frequency peaks that might refer to a certain component of the gearbox. Unfortunately, the peaks in this frequency spectrum cannot refer to a specific component.

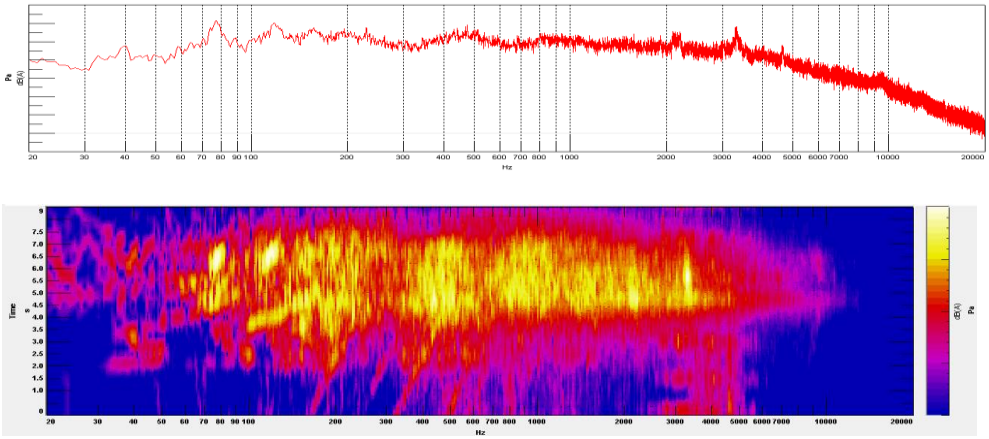

Figure 6

Averaged spectrum (top) and colormap (bottom) of the pass-by noise

The next analysis is based on the time signals in *Figure 5* (standstill measurements), the average FFT spectrums of the vibration signals were created. The curves are representing the almost the same curve progression, except in the frequency range of 400–1500 Hz. This difference is the result of the different impedance of the two measurement points. Point 1 (red curve) is located on a stiff part of the gearbox housing, point 2 (green curve) is located on softer part with lower impedance (on the side cover) of the gearbox housing.

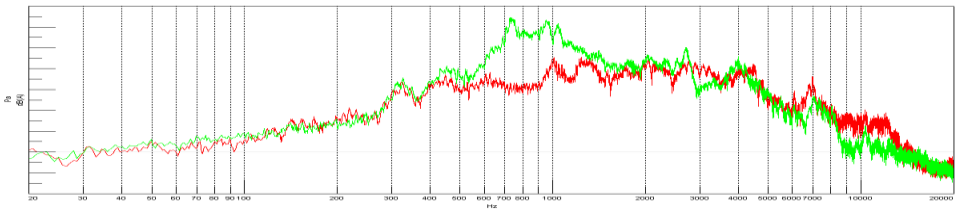

Figure 7

Averaged vibration spectrum at point 1 (red) and point 2 (green) on the gearbox housing

Figure 8 shows the comparison of noise spectrum in near field of the gearbox and vibration spectrum on the gearbox housing by the standstill measurements. In this case the curves have also almost the same progression, with some minor differences. It can be stated that the noise and vibration generated by the failure, on one hand will be transmitted through the wall of the gearbox housing, on the second hand the vibration is transferred to the housing and the housing is radiating the noise to the surrounding field. Unfortunately, also in this case the exact localisation of the failure is not possible.

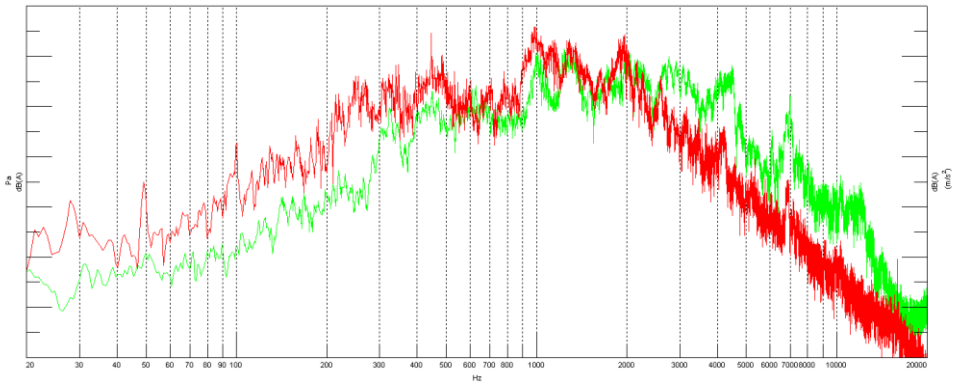

Figure 8
Averaged noise spectrum in near field (red) and averaged vibration spectrum at point 1 (red) on the gearbox housing

As shown before the noise and vibration analysis did not lead to the localization of the faulty component of the gearbox. For further analysis the study of the gearbox structure and later the disassembling of the gearbox could lead to the solution. The manual gearboxes containing a mechanism, which function is the moving certain gears into mesh position with other gears. This mechanism contains several shift rods (3 pcs. by a 6-speed manual gearbox) and shift forks. The rods are connected to the forks, and the forks are connected to the synchronizers. By the shift process triggered by the driver one of the shift rods (depending on which speed is shifted by the driver) is moving to its end position (shift position). In this shift mechanism in the gearbox a large clearance between some of the parts could be responsible for the generated impact noise. Another possible noise generation mechanism could be when the shift rod reaching its end position and an undamped impact happens.

5. CONCLUSIONS

It could be shown that acoustic methods through noise and vibration measurements, are not always capable to identify a specific problem in the car powertrain (and in general). If the generated noise and vibration of the specific failure are broadband, it is nearly impossible to make a proper failure detection. On the other hand, some of the failures generate very specific noise and vibration, with discrete frequency

contents. In this case the identification could be more sufficient, since the fault frequency refer exactly to the component, e.g., the meshing frequency of a gear pairing. In case of a broad band failure noise/vibration (as in current case study) only the localisation the unit (gearbox) which containing the faulty component might be possible, but it is not possible to exactly localize the faulty part. In this case unfortunately further analysis must be done, even the disassembly of the unit must be performed.

REFERENCES

[1] Nagyszokolyai I., Lakatos I. (2011). *Gépjárműdiagnosztika*. Egyetemi Tananyag, Kecskeméti Főiskola Gépipari Automatizálási Műszaki Főiskolai Kar, pp. 11–16.

[2] Denton, T. (2006). *Advanced Automotive Fault Diagnosis*. 2nd ed. Burlington, MA: Elsevier BH, pp. 63–64.

[3] Jayaswal, P., Aherwar A. (2012). Fault Detection and Diagnosis of Gear Transmission System via Vibration Analysis. *SSRN Scholarly Paper*, Rochester, NY: Social Science Research Network, July 2, 2012. https://papers.ssrn.com/abstract=2097703.

[4] Puchalski, A. (2015). A Technique for the Vibration Signal Analysis in Vehicle Diagnostics. *Mechanical Systems and Signal Processing*, 56–57 (May 1, 2015), pp. 173–80, https://doi.org/10.1016/j.ymssp.2014.11.007.

[5] Chen, J., Randall, R., Feng, N., Peeters, B., Auweraer, H. (2013). *Automated Diagnostics of Internal Combustion Engines Using Vibration Simulation*. Proceedings of the ICSV20, Bangkok.

[6] Hambric, S., A., Shung, H., S., Nefske, D., J. (2016). *Engineering vibroacoustic analysis: methods and applications.* Wiley Series on Acoustics, Noise and Vibration Series List, pp. 1–5.

[7] Jardine, A., Lin, D., Banjevic, D. (2006). A review on machinery diagnostics and prognosticsimplementing condition-based maintenance. *Mechanical Systems and Signal Processing*, 20, pp. 1483–1510.

[8] Kriston, J., B., Jálics, K. (1935). Application of vibro-acoustic methods in failure diagnostics. *Journal Of Physics-Conference Series*, 1, p. 012002 (2021).

Design of Machines and Structures, Vol. 11, No. 2 (2021), pp. 36–43.
https://doi.org/10.32972/dms.2021.013
http://orcid.org/0000-0002-9636-827 (Sz. Nagy)
http://orcid.org/0000-0001-8487-4327 (K. Jármai)
http://orcod.org/0000-0003-2727-2498 (A. Baksa)

EVOLUTIONARY OPTIMIZATION OF A TRANSMISSION LINE TOWER WITH FPA ALGORITHM

SZILÁRD NAGY[1] – KÁROLY JÁRMAI[2] – ATTILA BAKSA[3]

University of Miskolc,
[1,2]Institute of Energy Engineering and Chemical Machinery,
[3]Institute of Applied Mechanics
3515 Miskolc-Egyetemváros, Hungary
szilard.nagy@emerson.com, karoly.jarmai@uni-miskolc.hu,
attila.baksa@uni-miskolc.hu

Abstract: The optimization of the pylon is shown in this paper. The optimization is made by using flower pollination algorithm. The objective function is mass of the structure. The design constraints are static stress, local buckling and buckling. The unknowns are the typical dimensions of the circular hollow section truss. Parametric inspections have been made changing yield strength of material and the number of grid divisions. The results show that the use of higher yield strength steels, do not imply a lighter structure.

Keywords: *evolutionary optimization, finite element method, pylon, truss structure*

1. INTRODUCTION

Metaheuristic and nature inspired evolutionary algorithms are efficiently used for solving non-linear engineering problems, such as many dimensional optimization problems. Xin-She Yang proposed the flower pollination [4]. It is inspired by the reproduction process of plants. The Flower pollination algorithm like most evolutionary algorithms is developed for solving continuous, unconstrained optimization problems.

Usually transmission line towers, pylons are made from angle section trusses [1], [2]. The buckling stiffness of angle sections are very small. Orbán et al. [3] had shown the usage of a circular hollow section (CHS) is more favorable.
In this paper, we inspect whether the use of higher yield strength steel has additional beneficial effects for CHS.

2. FLOWER POLLINATION ALGORITHM [FPA]

Flower pollination is a major reproduction process of plants. It can take two forms, abiotic (local) and biotic (global). Pollens are transferred long distances during global pollination by pollinators such as insects, birds, wind, etc. This is specific to

about 90% of flowering plants. The Abiotic form does not require any pollinator. This inspired a method to develop FPA algorithm in [4].

In the FPA algorithm, global pollination is modelled by following equation

$$^{(G+1)}\mathbf{x}_{Gi} = {}^{(G)}\mathbf{x}_i + L\left({}^{(G)}\mathbf{x}_i - {}^{(G)}\mathbf{g}_*\right) \tag{1}$$

where (G) is G[th] generation, $\mathbf{x}_i$ is i[th] individual in population, L is a Levy distribution random number and $\mathbf{g}_*$ represents the fittest individual in a population. Local pollination can be described

$$^{(G+1)}\mathbf{x}_{Li} = {}^{(G)}\mathbf{x}_i + \epsilon\left({}^{(G)}\mathbf{x}_j - {}^{(G)}\mathbf{x}_k\right) \quad i \neq j \neq k \tag{2}$$

where ϵ is a uniform distribution random number in $[0,1]$ interval and j, k are random indicies. A p probability variable decides between the two mutation methods. A more detailed description and complete algorithm can be found in [4]

$$^{(G+1)}\mathbf{x}_i = \begin{cases} {}^{(G+1)}\mathbf{x}_{Gi} & p \leq \mathrm{rand}[0,1) \\ {}^{(G+1)}\mathbf{x}_{Li} & \text{otherwise} \end{cases} \tag{3}$$

3. INSPECTED PYLON WITH THEIR LOADS

In the present case, the subject of the investigation is a 45 m high intermediate pylon. The structure can be divided into two parts, a 21 m high top and a 24 m high bottom. The loads were according to [5]. The size-giving load is half a wire pull. Without detailing the calculations from [1] forces transmitted from the upper pylon part are $F_V = 209.03\,\mathrm{kN}$ vertical force, $F_H = 312.14\,\mathrm{kN}$ horizontal force and $M_h = 2850.5\,\mathrm{kNm}$ bending moment. In the load calculations 400 m span length, weight of 12 pieces wire and 1.1 safety factor are applied.

Forces reduced to vertices as shown in

$$F_{y1} = \frac{M_h}{2a_2} - \frac{F_v}{4} = \frac{2850.5\,\mathrm{kNm}}{2 \cdot 3.7\,\mathrm{m}} - \frac{209.03\,\mathrm{kN}}{4} = 332.94\,\mathrm{kN} \tag{4}$$

$$F_{y2} = \frac{M_h}{2a_2} + \frac{F_v}{4} = \frac{2850.5\,\mathrm{kNm}}{2 \cdot 3.7\,\mathrm{m}} + \frac{209.03\,\mathrm{kN}}{4} = 437.46\,\mathrm{kN} \tag{5}$$

where $a_2 = 3{,}7\ m$ is the width of the upper pylon part. It is sufficient to perform the calculations on only one inclined plane relevant to the loads as shown on . In the case of a pyramid with a side skew of $\beta = 80°$, the forces acting on the inclined plane under investigation, as indicated in

$$F_1 = \frac{F_{y1}}{\sin\beta} = \frac{332.94\,\mathrm{kN}}{\sin 80°} = 338.08\,\mathrm{kN} \tag{6}$$

$$F_2 = \frac{F_{y2}}{\sin\beta} = \frac{437.46\ \text{kN}}{\sin 80°} = 444.21\ \text{kN} \tag{7}$$

$$F_3 = \frac{F_h}{2} = \frac{312.14\ \text{kN}}{2} = 338.08\ \text{kN} \tag{8}$$

illustrates an example with a grid of $n_g = 2$. During further investigations, several grid division tasks will be solved. Grid divisions are reduced or increased based on the following relationship

$$h_1 = \frac{h}{2.5 n_g} \tag{9}$$

Trusses of the planar truss model were classified into three cross-sectional groups. The first group consists of the elements of the side column (1–10 trusses). Members of the second group are horizontal elements (17–22 trusses). Finally, the third group consists of grid elements forming a deltoid and a triangle (23–26 trusses). In each cross-section group, the circular section is used, the characteristic dimensions of which are shown in *Figure 3*

Cross-section of circular tube. Such as outer diameters D_1, D_2, D_3 and wall thicknesses t_1, t_2, t_3.

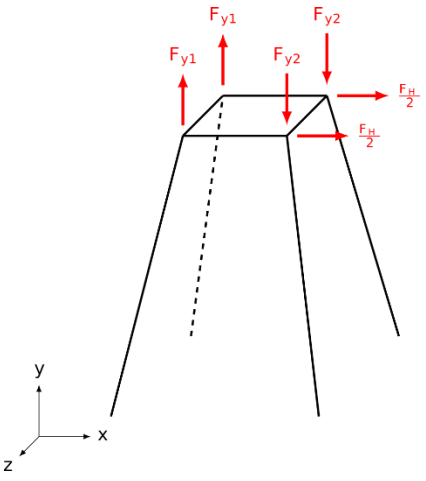

Figure 1
Sketch of lower part of pylon

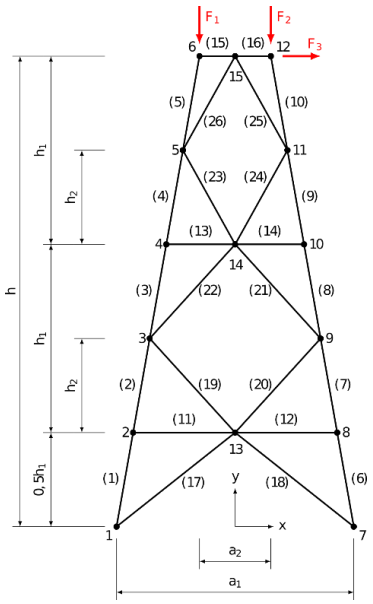

Figure 2
Planar truss structure

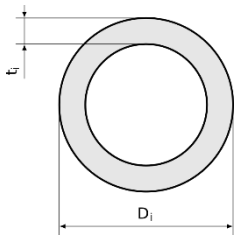

Figure 3
Cross-section of circular tube

4. APPLIED FINITE ELEMENT MODEL

In this case the planar structure could be modelled as a pushed and pulled truss model, as shown in *Figure 4*.

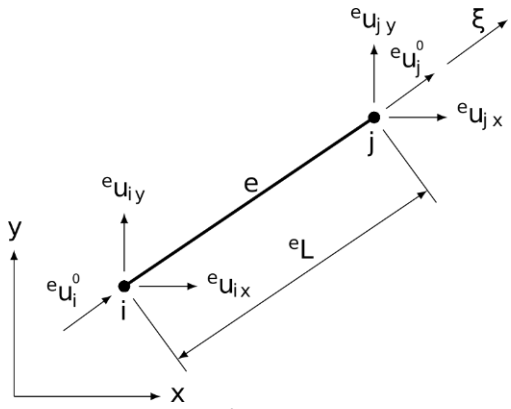

Figure 4
Finite element model of truss

Node displacement is only possible along the ξ axis (local coordinate system) passing through nodes i and j. In the *x-y* global coordinate system, the *x*, *y* projections of this displacement are interpreted

$$^{e}\mathbf{u}' = \left[^{e}u_i' \quad ^{e}u_j'\right]^{T} \qquad ^{e}\mathbf{u} = [^{e}u_{ix} \quad ^{e}u_{iy} \quad ^{e}u_{jx} \quad ^{e}u_{jy}]^{T} \tag{10}$$

The transition between the two coordinate systems is possible with the transformation matrix

$$^{e}\mathrm{T} = \begin{bmatrix} ^{e}T_{11} & ^{e}T_{12} & 0 & 0 \\ 0 & 0 & ^{e}T_{23} & ^{e}T_{24} \end{bmatrix} \tag{11}$$

$$^{e}T_{11} = {}^{e}T_{23} = \frac{^{e}u_{jx} - {}^{e}u_{ix}}{^{e}L} \qquad ^{e}T_{12} = {}^{e}T_{24} = \frac{^{e}u_{jy} - {}^{e}u_{ix}}{^{e}L} \tag{12}$$

In equilibrium, the total Π potential energy is minimal, that is mean the $\delta\Pi$ first variation of potential energy is zero for whole structure. The total potential energy for elements is depicted in the local and then global coordinate system

$$ {}^{e}\Pi' = \frac{1}{2} \cdot {}^{e}\mathbf{u}'^{T} \cdot ({}^{e}\mathbf{K}' \cdot {}^{e}\mathbf{u}' - {}^{e}\mathbf{f}') \tag{13} $$

$$ {}^{e}\Pi = \frac{1}{2} \cdot {}^{e}\mathbf{u}^{T} \cdot ({}^{e}\mathbf{K} \cdot {}^{e}\mathbf{u} - {}^{e}\mathbf{f}) \tag{14} $$

where **f** is a generalized loads vector reduced to nodes, and $\mathbf{K}'$, **K** are the stiffness matrices in local and global coordinate systems

$$ {}^{e}\mathbf{K}' = \frac{{}^{e}E \cdot {}^{e}A}{{}^{e}L} \begin{bmatrix} 1 & -1 \\ -1 & 1 \end{bmatrix} \tag{15} $$

$$ {}^{e}\mathbf{K} = {}^{e}\mathbf{T}^{T} \cdot {}^{e}\mathbf{K}' \cdot {}^{e}\mathbf{T} \tag{16} $$

Introducing **u** vector of nodal displacements and **f** load vectors of the total system potential energy

$$ \mathbf{u} = [{}^{1}\mathbf{u} \quad {}^{2}\mathbf{u} \quad {}^{3}\mathbf{u} \quad \cdots \quad {}^{e}\mathbf{u}]^{T} \qquad \mathbf{f} = [{}^{1}\mathbf{f} \quad {}^{2}\mathbf{f} \quad {}^{3}\mathbf{f} \quad \cdots \quad {}^{e}\mathbf{f}]^{T} \tag{17} $$

$$ \delta\Pi = 0 = \frac{1}{2}\delta\mathbf{u}^{T}(\mathbf{K}\mathbf{u} - \mathbf{f}) \tag{18} $$

where **K** is the stiffness matrix of the whole system, the elements of this must be determined according to the rules of element fitting [6]–[8]. Also, the boundary conditions should be applied to (18) equation. A non-trivial solution of (18) exists only if the term in parentheses is zero.

Stress of elements could be calculated from the nodal displacement vector

$$ {}^{e}\sigma = \frac{{}^{e}E}{{}^{e}L} \cdot [-{}^{e}T_{11} \quad -{}^{e}T_{12} \quad {}^{e}T_{11} \quad {}^{e}T_{12}] \cdot {}^{e}\mathbf{u} \tag{19} $$

5. THE OPTIMIZATION PROBLEM

During the optimization, the minimal mass of the structure was searched

$$ \min\left(\sum_{i=1}^{n_e} m_i\right) = \min\left(\rho \sum_{i=1}^{n_e} A_i L_i\right) \tag{20} $$

where m_i is the mass of elements, A_i is the cross-sectional area of elements, L_i is length of elements and ρ is the density of elements. This optimization is a constrained optimization because the structure must meet strength and stability requirements. In the present case, three criteria have been considered, such as resistance to tensile, buckling, and local buckling. These constraints can be well characterized by the cross-sectional utilization factors.

The first constraint of each element contains the resistance to tensile and buckling

$$g_{Ii} = \begin{cases} \dfrac{\gamma_{M0}|^{e}\sigma|}{\chi f_y} & {}^{e}\sigma < 0 \\ \dfrac{\gamma_{M0}|^{e}\sigma|}{f_y} & {}^{e}\sigma \geq 0 \end{cases} \tag{21}$$

where f_y is the yield strength, γ_{M0} is the generalized safety factor according to [9], and χ is the buckling factor according to [9]. If the stress is less than zero, that means the load is pushing, otherwise the load is pulling. Second constraints of each element come from criteria of local buckling. Recommendations of [9] for diameter and wall thickness ratio of circular hollow section

$$g_{IIi} = \frac{D_i f_y}{21150 t_i} \tag{22}$$

Equation (22)(22) is true only if the unit of f_y yield strength is MPa, and the unit of D_i, t_i dimensions are mm. The value of g_{Ii} must be calculated for each truss, while g_{IIi} is sufficient only once for each cross-sectional group.

According to previously described equations the fitness function of optimization

$$\mathcal{F}(D_1, D_2, D_3, t_1, t_{2,} t_3) = \sum_{i=1}^{n_e} m_i + \sum_{i=1}^{n_e} p_{Ii} + \sum_{i=1}^{3} p_{IIi} \tag{23}$$

where p_{Ii} and p_{IIi} are the "death" penalty functions

$$p_{Ii} = \begin{cases} 0 & g_{Ii} \leq 1 \\ 10^6 g_{Ii} & g_{Ii} > 1 \end{cases} \tag{24}$$

$$p_{Ii} = \begin{cases} 0 & g_{Ii} \leq 1 \\ 10^6 g_{IIi} & g_{IIi} > 1 \end{cases} \tag{25}$$

6. RESULTS OF OPTIMIZATION

During the optimization, more grid divisions $n_g = 1 \cdots 6$ are investigated, with different base materials. The yield strength of the inspected structural steels varied

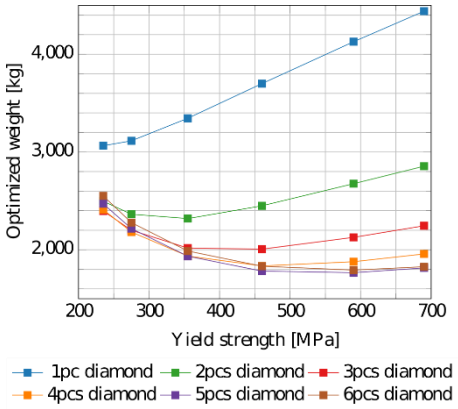

Figure 5
Optimized weight

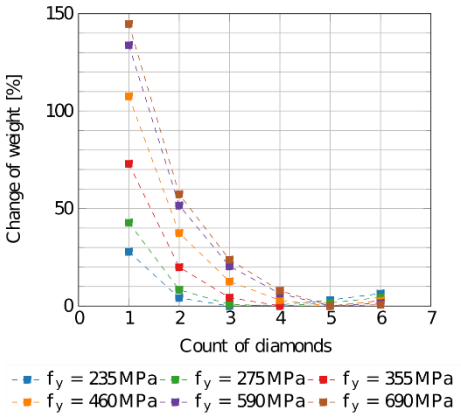

Figure 6
Percentage change in optimized weight

between 235 MPa and 690 MPa. During running of optimization, the fitness function was converging continuously to a minimum value.

Results of optimization shown in *Figure 5* and *Figure 6*. As can be seen, the use of higher yield strength steel does not clearly result in a lighter structure. The number of grid divisions should also increase to achieve less weight. An increase in yield strength on one side improves the overall resistance of the element, but on the other hand worsens the buckling factor. The optimal result is obtained when these two effects are balanced. In this case the optimal result is when yield strength is $f_y = 460$ MPa and number of grid divisions is $n_g = 5$.

7. CONCLUSIONS

The combination of flower pollination algorithm and finite element method is efficiently used for optimizing truss like structures. In this case optimizing the lower part of a pylon. The iterative calculation process is easy to automate and does not require derivatives that are difficult to produce. The presented method can be easily adopted to solve other truss problems as well.

The results of optimization show that, usage of higher strength steel dose not contribute to a lighter structure without changing the topology.

ACKNOWLEDGEMENT

The research was supported by the Hungarian National Research, Development and Innovation Office—NKFIH under the project number K 134358.

REFERENCES

[1] Rao, G. V. (1995). Optimum design for transmission line towers. *Computers & Structures*, Vol. 57, No. 1, pp. 81–92.

[2] Silva, J. G. S., Vellasco, P. C. G., Andrade, S. A. L., Oliveira, M. I. R. (2005). Structural steel design and behaviour; Steel structures; Spatial structures; Telecommunication and transmission towers. *Journal of Constructional Steel Research*, Vol. 61, No. 8.

[3] Orbán, F., Farkas, J., Jármai, K. (2011). Optimum design of a transmission line tower : Welded tubular truss structure. *6th European Conference on Steel and Composite Structures*, Eurosteel 2011, Brussels.

[4] Yang, X. S. (2012). *Flower pollination algorithm for global optimization, Unconventional Computation and Natural Computation*. Springer Berlin Heidelberg, Berlin.

[5] MSZ 151-1:2000 (2000). *Power overhead lines. Installation requirements for overhead lines with a nominal voltage greater than 1 kV*. Magyar Szabványügyi Testület, Budapest (in Hungarian).

[6] Páczelt, I. (1999). *Finite element method in engineering practice*. Miskolci Egyetemi Kiadó, Miskolc (in Hungarian).

[7] Ferreira, A. J. M. (2009). MATLAB Codes for Finite Element Analysis. Springer Netherlands, Amsterdam.

[8] Smith M. I.; Lee M.; Programming the Finite Element Method, 4th edition, ISBN 0-470-84969-3, John Wiley and Sons Ltd, London, 2004

[9] EN 1993-1-1:2009; Eurocode 3: Design of steel structures - part 1-1: General rules and rules for buildings, European Committee Standardization, Brussels, 2009.

Design of Machines and Structures, Vol. 11, No. 2 (2021), pp. 44–58.
https://doi.org/10.32972/dms.2021.014
http://orcid.org/0000-0001-9230-4949 (L. Trautmann)

PRINCIPLES OF NATURE IN PRODUCT DESIGN

LAURA TRAUTMANN

Department of Machine and Product Design
Faculty of Mechanical Engineering
Budapest University of Technology and Economics
Műegyetem rkp. 3, H-1111, Budapest, Hungary
E-mail: trautmann.laura@gt3.bme.hu

Abstract: Product designers should pay attention to many attributes of a product during design, however, studies have shown that besides the functionality, the aesthetically-pleasing appearance of products attracts consumers, and it has a significant effect on the buying process. Thus, it is efficient to know what geometries, colours, materials, etc., are pleasing to the human eye. This article deals with geometries that appear in nature since these forms are pleasing to many people of different generations and cultures and provide a sense of harmony. The hypothesis is that the usage of the mathematically describable principles of nature – such as Fractals, Golden Ratio, Fibonacci Sequence, Voronoi Diagram – could result in a better-looking design that increases the success of the product, like in the cases of Stradivarius violin, Aston Martin, or Apple logo.

Keywords: *Product design, Nature-inspired design, Mathematics in design, Geometry, Aesthetics*

1. INTRODUCTION

Nowadays, there are many design methods and principles for product designers. Designers should pay attention to the product life cycle, the sustainable material choice, the user experience, the practical and user-friendly design, etc. That is why design education is about to face interdisciplinary challenges [1, 2], where continuous support and development is necessary.

There is no one rule of successful design, however, there are some fascinating facts about the most successful products, which could show that besides many factors, beauty and harmony have a massive impact on us, as Donald Norman said: "Attractive things work better." [3, 4] Other studies [5–9] have also shown that the factor of beauty or aesthetics is an essential criterion of the quality of design.

Forms appearing in nature are aesthetically-pleasing to the human eye and provide satisfaction and harmony by their proportion. That is why some researchers already tried to gain inspiration from nature while designing objects [10]. The hypothesis is that if designers implement the beauty of nature in their design, it could bring more success. This article introduces examples of the forms in nature with mathematical

explanations and connected examples of arts since art and design have the same goal by attracting consumer attention. Although art and design could be affected by nature and mathematical objects on many levels, this article deals with Fractals, Golden Ratio, Fibonacci Sequence and Voronoi Diagram. Besides that, nature forms inspired product examples introduced in this paper prove that the usage of these geometries can be principles in the field of design and could bring more success for designers and engineering designers.

2. FRACTALS

Fractal is a self-similar geometry that develops through iterations. The name "fractal" originates from the "fractus" Latin word, which means broken, unsmooth. It was introduced by Benoit Mandelbrot in 1976, however, the mathematical history of fractal goes back to the 19 century. One of the main milestones of this journey was in 1904 when Helge von Koch defined the Koch curve. In *Figure 1*, a few iterations can be seen, where the process begins with a unit length line. At the first iteration, the center is extracted and replaced with two lines with 1/3 length, at 60° angle. The process is continuing with an infinite number of iterations [11, 12].

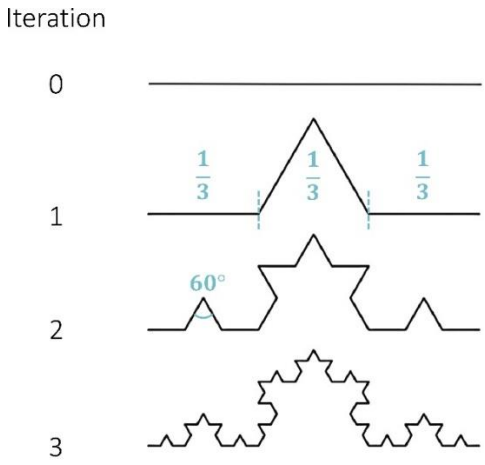

Figure 1
Koch curve at iterations from 0 to 3

With fractal, Mandelbrot could describe natural phenomena.

"Why is geometry often described as 'cold' and 'dry'? One reason lies in its inability to describe the shape of a cloud, a mountain, a coastline, or a tree. Clouds are not spheres, mountains are not cones, coastlines are not circles, and bark is not smooth, nor does lightning travel in a straight line. Nature exhibits not simply a higher degree but an altogether different level of complexity." Benoit Mandelbrot [13]

Figure 2 presents a few examples of fractal appearance in nature. Among others, fractal – the self-similar geometry – can be discovered in peacock feathers, lake (on the collage: Lake Nasser, Egypt) tentacle, eyes, cauliflower, and leaves as well.

Figure 2
Fractal appearance in nature: peacock feathers [14],
Lake Nasser, tentacle, eyes, roman cauliflower, and leaves [15]

In the 1980s – parallel to technical innovations – fractal geometry became displayable, which opened up a new world for both mathematicians and artists. Among the branches of fine arts, we may already speak of a separate fractal art where software creators are able to produce similar images shown in *Figure 3* with software support.

Figure 3
Examples of fractal arts: a collection of works by artists from a site called DeviantArt [16]

Fractals – among others – are appearing on clothing design, website design, and architecture as well. In order to show some architectural examples, in *Figure 4* a ceiling in Iran [17], the Sky Habitat for Singapore designed by Moshe Safdies [18], and the wall of the Centenary of the Federation of Australian States [11] can be seen.

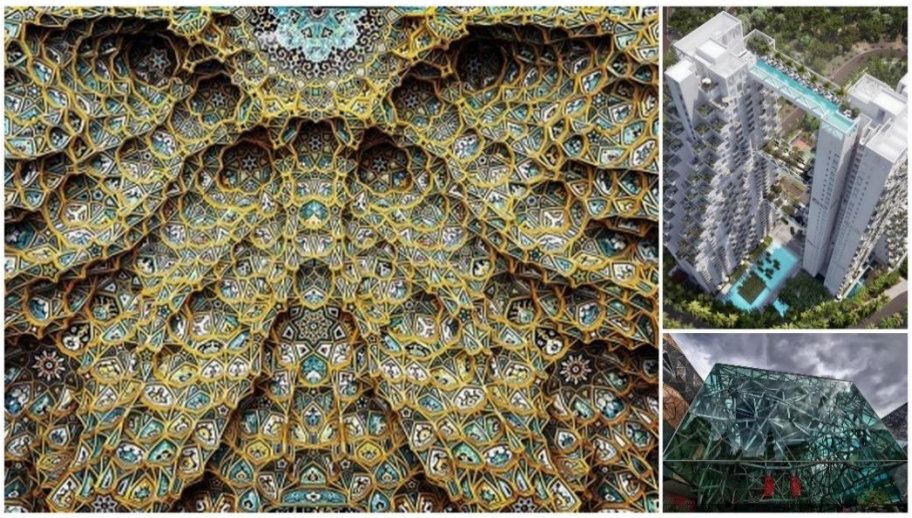

Figure 4
Fractal in architecture: Ceiling in Iran [17],
the Sky Habitat for Singapore designed by Moshe Safdies [18],
the wall of the Centenary of the federation of Australian States [11]

3. GOLDEN RATIO

The origin of fractal geometry is derived from ancient Greek philosophers, just like other ratios-systems. Among one of them is the Golden Ratio that is widely considered to be the most perfect and beautiful proportion. The Golden Ratio *(Figure 5)* means that the longer segment "a" is proportional to the shorter segment "b", at the same rate, the sum of "a" and "b" is proportional to the "a" segment [19]. If "a" the longer segment and "b" is called the shorter, the proportion may be described by:

$$a : b = (a + b) : a = 1.6180339887(\text{approx.}) \quad (1)$$

$$\frac{a}{b} = \frac{a+b}{a} = 1.6180339887$$

Figure 5
Explanation of Golden Ratio

Golden Ratio can be found in nature, in architecture, in design, in engineering, in arts as well [20–22]. Golden Ratio is appearing of the human body, for instance, on the human face (length of face/width of face, length of mouth/width of nose and so on), on the human hand (e.g., the proportion of the first two to the full length of the finger), on human lungs, on the hearing and balance organ, on the cardias cycle and even on the brain waves [23]. *Figure 6* presents a few proportions of the human body.

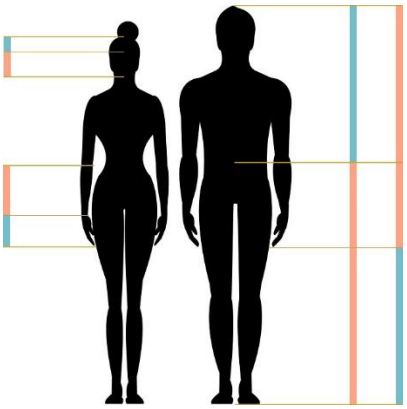

Figure 6
Golden proportion of human body

Since Golden Ratio is very pleasing for the eye and provides harmony, it is commonly used in the design of art. *Figure 7* shows an example of Leonardo Da Vinci's pictures, The Last Supper. The dimensions of the room were created by the usage of the Golden Ratio.

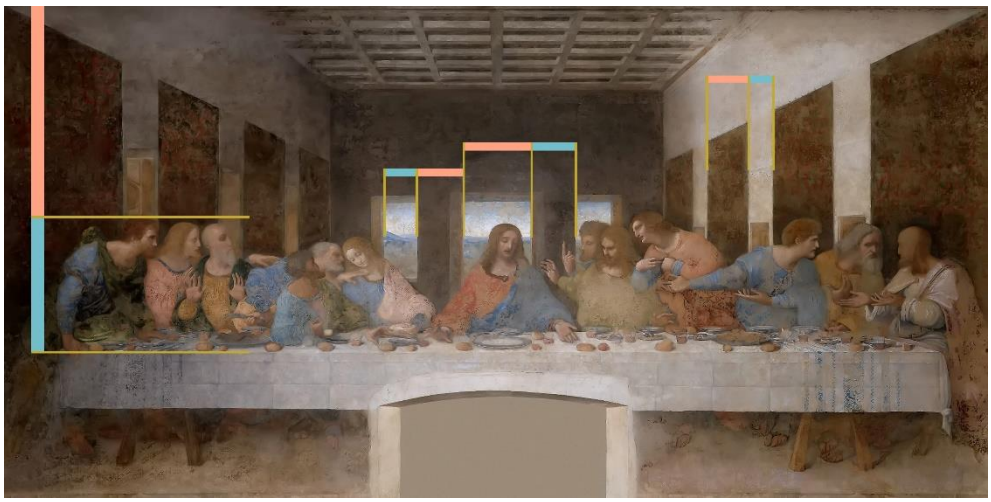

Figure 7
The Last Supper based on Golden Ratio

In *Figure 8*, a Golden Ratio inspired violin can be seen. It was designed by Antonio Stradivari, which is the most valuable string-playing instrument in the world because of its harmonic qualities [24, 25]. (It is sold for nearly 16M dollar.)

Figure 8
Stradivarius violin based on Golden Ratio

Golden Ratio also found in car designs such as Volkswagen Beetle [20] or Aston Martin [26] as in *Figure 9*. The Aston Martin DB9 is described as:

"Perfectly Proportioned – Every inch of DB9's form is designed for elegance and balance. The simple beauty of nature guides the design of DB9, with the 'golden ratio' setting all proportions. The result is a profile where every line, dimension and proportion works in harmony. Combine this with the near perfect weight distribution, provided by a lower engine placement, and you have a DB9 balanced on sight and in experience." [26, 27]

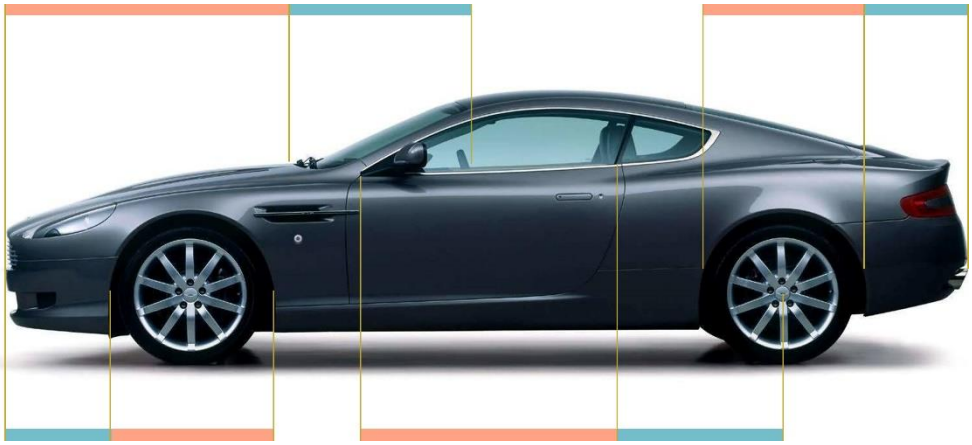

Figure 9
Example of car design based on Golden Ratio

4. FIBONACCI SEQUENCE

A similar arithmetic approach is the Fibonacci Sequence, named after the Italian mathematician Leonardo Fibonacci. Fibonacci Sequence: Starting with the beginning of the sequence, we inscribe a series of numbers where the next member is always composed of the sum of the two preceding members. The sequence of the numbers is: 0, 1, 1, 2, 3, 5, 8, 13, 21, 34, 55, 89, 144, 233, 377, 610, 987, 1597, 2584, … etc. [28, 29] *(Figure 10)*. The quotient of the series is approaching to the number of golden ratio: ~1.618...

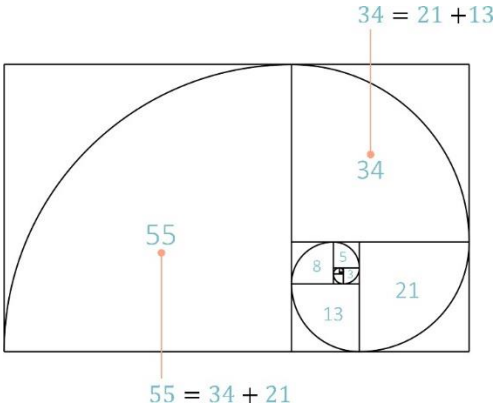

Figure 10
Explanation of Fibonacci Sequence

This sequence can be seen widely in the natural world, for example, in seahorse, plants, flowers, storms, snail, and so on *(Figure 11)*.

Figure 11
Nature creation examples of Fibonacci Sequence: seahorse [30], *carnivorous plant* [31], *sunflower* [32], *hurricane* [33], *calla lily* [34], *cuban snail* [35]

For an example of art, a rhythm of Béla Bartók can be mentioned *(Figure 12)*. Many composers used Fibonacci numbers and Golden Ratio in their composition in order to provide a formal structure of them [36].

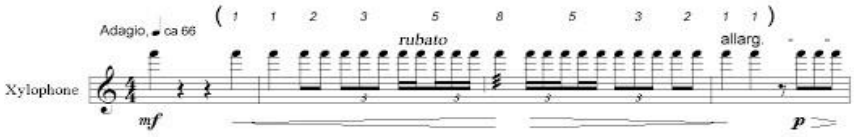

Figure 12
A palindromic rhythm based on Fibonacci numbers in the opening of the third movment by Béla Bartók [36]

As shown in *Figure 13*, the Apple logo is based on the Fibonacci Sequence. It is designed by Paul Rand, who is an American graphic designer with a successful career in the field of logos [37]. (He has references in IBM, UPS, Enron, Westinghouse, ABC, and Steve Jobs' NeXT as well.)

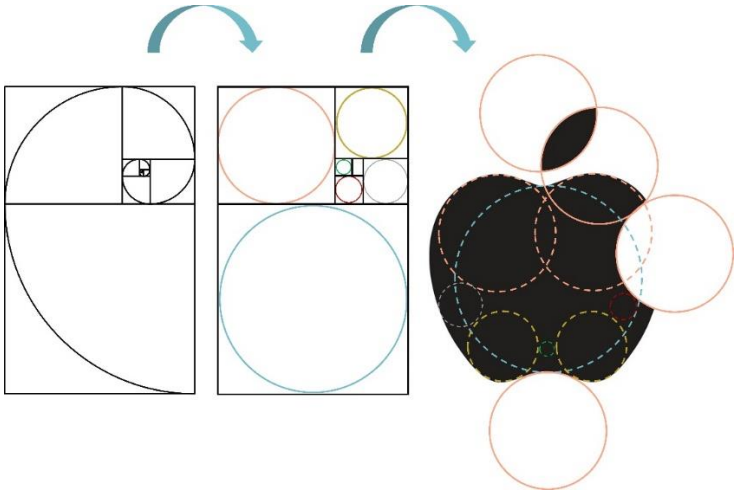

Figure 13
Apple logo, based on the Fibonacci Sequence

5. VORONOI DIAGRAM

Voronoi Diagram is an algorithmic diagram that was formulated by a Ukrainian mathematician Georgy Voronoy (1868–1908). (The concept was only published in the year of his death [38].)
When introducing the Voronoi Diagram, we use the concept of distance. In this article, we will work with the Euclidean distance. Denote the Euclidean distance between points $p(p_x, p_y)$ and $q(q_x, q_y)$ by $d(p,q)$.
Then

$$d(p,q) = \sqrt{(p_x - p_y)^2 + (q_x - q_y)^2} \tag{2}$$

Let $P = \{p_1, p_2, \ldots, p_n\}$ be a set containing n different points in the plane. The Voronoi diagram of P is interpreted as the division of the plane into n cells (ranges), with the property that a point q belongs to a cell belonging to point p_i if and only if

$$d(q, p_i) < d(q, p_j) \ \forall p_j \in P, j = i \tag{3}$$

Denote the Voronoi diagram of of P: *Vor(P)*.

The cell belonging to p_i is denoted by *V(i)* and is called the Voronoi cell of p_i. Based on the interpretation of the Voronoi Diagram, this cell has the property that the points inside it, among the points P are closest to p_i [39, 40].

The cells can be formed by section bisector set on lines drawn between the points *(Figure 14a, b, c)*. A plane shape is the set of points closest to the examined point from the available points *(Figure 14d)*. The cells of the Voronoi mesh are complex polygons in the plane *(Figure 14e*) or complex polyhedra in space.

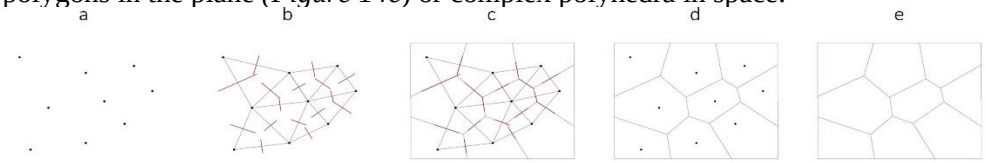

Figure 14
Explanation of the Voronoi Diagram

This mathematical model appears as natural patterns in many phenomena. To show some examples, in *Figure 15*, we can see a honeycomb, giraffe skin, sea turtle, dry earth, dragonfly wing, and soap bubble.

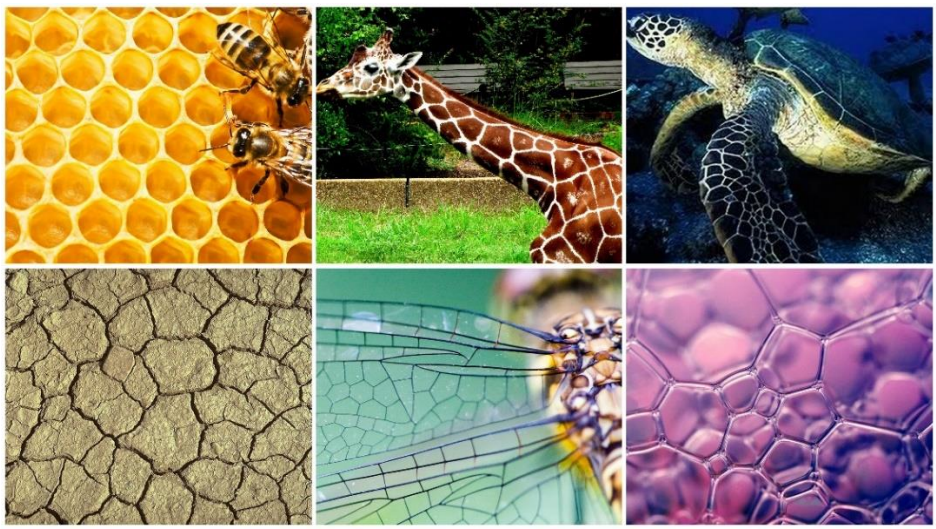

Figure 15
Voronoi Diagram appearance in nature: honeycomb [41], *giraffe skin* [42], *sea turtle* [43], *dry earth* [44], *dragonfly wing* [45], *and soap bubble* [46]

The Voronoi Diagram is also used in many cases in art. For example, it is possible to create mosaic images or portraits by its help as illustrated in *Figure 16*.

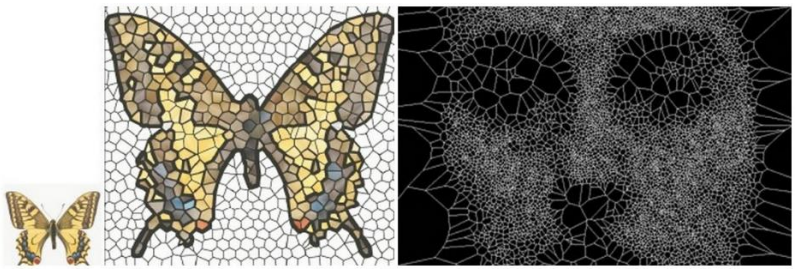

Figure 16

Application of Voronoi Diagrams in Arts: An example of an automatic method for mosaicing images by using Voronoi diagrams: the input image (left) and the result image (right) [47]*; Portrait called Segmentation and Symptom by Golan Lenin* [48]

The application of the Voronoi Diagram is widespread among architects and product designers. For instance, *Figure 17* shows the 2011 Millennium Yacht Design Award winner, the extravagant 125-meter superyacht called Voronoi created by Kim Hyun-Seok, a South Korean industrial architect. The designer said that this lattice exterior provides harmony with its natural appearance [49]. *Figure 17* also shows the Voronoi Chair designed by Franken Architekten. The cellular form of wood is based on the Voronoi Diagram. The chair is created from a cluster of spatial cells that behave similarly to the Voronoi cell structure. The designer writes that the cellular covers establish a feeling of balanced proportions [50].

Figure 17

Voronoi Diagram inspired superyacht [51] *and chair* [50]

6. CONCLUSION

With the development of science, scientists could describe the phenomena of nature better and better. This knowledge is useful for product designers as well, not only because mathematical concepts are not far from design concepts (such as symmetry, pattern and so on), but also the beauty and harmony of nature can be implemented in the design, as it is shown in case of many successful products in the past.

These examples have proved that if designers consider these principles during the concept-development of the product design process, the solution could bring more success.

ACKNOWLEDGEMENT

The research reported in this paper and carried out at BME has been supported by the NRDI Fund (TKP2020 NC, Grant No. BME-NCS) based on the charter of bolster issued by the NRDI Office under the auspices of the Ministry for Innovation and Technology.

REFERENCES

[1] Huang, X., Ball, R., Wang, W. (2020). Comparative study of industrial design undergraduate education in China and USA. *International Journal of Technology and Design Education*, pp. 1–22. http://doi.org/10.1007/s10798-020-09563-4.

[2] Costa Junior, J. da, Diehl, J. C., Secomandi, F. (2018). Educating for a systems design approach to complex societal problems. *Journal ofEngineering Design*, 29, pp. 65–86, http://doi.org/10.1080/09544828.2018.1436162.

[3] Norman, D. (2002). Emotion & design: attractive things work better. *interactions*, *9*, pp. 36–42. http://doi.org/10.1145/543434.543435.

[4] Hohl, M. (2009).Beyond the screen: visualizing visits to a website as an experience in physical space. *Visual Communication*, 8, pp. 273–284.

[5] Qu, Y., Mao, X., Li, D. (2018). Research on the Role of Design Aesthetics in Modern Design. *MATEC Web of Conferences. EDP Sciences*, Vol. 176, p. 02012, http://doi.org/10.1051/matecconf/201817602012.

[6] Mata, M. P., Ahmed-Kristensen, S., Brockhoff, P. B., Yanagisawa, H. (2017). Investigating the influence of product perception and geometric features. *Research in Engineering Design*, *28*, pp. 357–379, http://doi.org/10.1007/s00163-016-0244-1.

[7] Xenakis, I., Arnellos, A. (2013). The relation between interaction aesthetics and affordances. *Design Studies*, 34, pp. 57–73, http://doi.org/10.1016/j.destud.2012.05.004.

[8] Park, M. K., Lim, K. J., Seo, M. K., Jung, S. J., Lee, K. H. (2014). Spatial augmented reality for product appearance design evaluation. *Journal of Computational Design and Engineering*, *2*, pp. 38–46, [https://academic.oup.com/jcde/article-pdf/2/1/38/33133446/j.jcde.2014.11.004.pdf]. http://doi.org/10.1016/j.jcde.2014.11.004.

[9] Singh, R., Seniaray, S., Saxena, P. (2020). A Framework for the Improvement of Frugal Design Practices. *Designs*, 4, p. 37.

[10] Fu, Q., Chen, X., Su, X., Fu, H. (2016). Natural lines inspired 3D shape redesign. *Graphical Models*, 85, pp. 1–10.

[11] Belma, A., Sonay, A. (2016). Fractals and Fractal Design in Architecture. *13th International Conference "Standardization, Protypes and Quality: A Means of Balkan Countries' collaboration*", Vol. 17, pp. 282–291.

[12] Benyetho, T., El Abdellaoui, L., Zbitou, J., Bennis, H., Tribak, A., Latrach, M. (2017). A new dual band planar fractal antenna for UMTS and ISM bands. *Int. J. Commun. Antenna Propag. (I. Re. CAP)*, *7*, pp. 64–71, http://doi.org/10.15866/irecap.v7i1.11261.

[13] Mandelbrot, B. B. (1982). *The Fractal Geometry of Nature*. W. H. Freeman and Company, San Francisco, 1982.

[14] McNally, J. (2010). Earth's Most Stunning Natural Fractal Patterns. *Wired*. https://www.wired.com/2010/09/fractal-patterns-in-nature/.

[15] TechnoCrazed. (2013). Incredible Examples Of Fractals Found In Nature (Photo Gallery). *TechnoCrazed*. https://www.technocrazed.com/incredible-examples-of-fractals-found-in-nature-photo-gallery.

[16] DeviantArt. (2020). Discover The Largest Online Art Gallery and Community.

[17] Urbanist. (2016). Fractal Architecture: 14 Intricate Ceilings of Historic Iran. *Web Urbanist, Architecture, Art, Design & Built Environments*. https://weburbanist.com/2016/03/17/fractal-architecture-14-intricate-ceilings-of-historical-iran/.

[18] Rogers, S. (2014). Algorithmic Architecture: 14 Complex Math-Based Structures. *Web Urbanist, Architecture, Art, Design & BuiltEnvironments*. https://weburbanist.com/2014/02/26/algorithmic-architecture-14-fractalparametric-structures/.

[19] Hegde, P. (2017). Golden Ratio : What It Is And Why Should You Use It In Design. *Prototypr*. https://blog.prototypr.io/golden-ratio-what-it-is-and-why-should-you-use-it-in-design-7c3f43bcf98.

[20] Akhtaruzzaman, M., Shafie, A. A. (2011). Geometrical substantiation of Phi, the golden ratio and the baroque of nature, architecture,design and engineering. *International Journal of Arts*, 1, pp. 1–22, http://doi.org/10.5923/j.arts.20110101.01.

[21] Meisner, G. (2014). Golden Ratio in Art Composition and Design. *Golden Number*. https://www.goldennumber.net/art-composition-design/.

[22] Dömötör, Cs.; Péter, J. (2012). Design principles in nature. *Design of Machines and Structures*, 2, pp. 33–42.

[23] Murali, S. (2012). *Golden ratio in human anatomy*. Department of Science and Technology, http://doi.org/10.13140/2.1.2265.9526.

[24] Shannon, A. G., Klamka, I., Gend, R.v. (2018). Generalized Fibonacci Numbers and Music. *Journal of Advances in Mathematics, 14*, pp. 7564–7579, http://doi.org/10.24297/jam.v14i1.7323.

[25] Jafari, S., Karbasbaf, M. M. (2017). A Geometrical Method for Sound-Hole Size and Location Enhancement in Lute Family Musical Instruments: The Golden Method. *Arts*, Multidisciplinary Digital Publishing Institute, Vol. 6, p. 20.

[26] Meisner, G. (2014). Aston Martin, James Bond and the Golden Ratio. *Golden Number*. https://www.goldennumber.net/aston-martin-golden-ratio/.

[27] Aston Martin, W.D. DB9 - The World's Most Timeless Sports GT., 2020, https://www.astonmartinwashingtondc.com/?models=db9.

[28] Asharul Khan, D. C. G. (2014). Exploring the Fibonacci Sequence. *Dream 2047*, 17, pp. 30–32.

[29] Mundi, F. L. A. (2014). The Golden Ratio in classical music composition. *Zero equals two*. https://zeroequalstwo.net/the-golden-ratio-in-classical-music-composition/.

[30] Oktaviani, A. N. (2020). Ajak Anak Mencintai Laut dengan Mengenalkan 9 Binatang Laut Ini. *Orami*. https://www.orami.co.id/magazine/ajak-anak-mencintai-laut-dengan-mengenalkan-9-binatang-laut-ini/.

[31] Sierzputowski, K. (2014). Joni Niemelä's Macro Photographs Capture Carnivorous Plants' Alien-Like Structures. *Colossal*. https://www.thisiscolossal.com/2015/07/carnivorous-plants-joni-niemela/.

[32] Figure, G. (2014). Fibonacci in Natures. *Go Figure*. https://gofiguremath.org/natures-favorite-math/fibonacci-numbers/fibonacci-in-nature/.

[33] Myers, S. Patterns, (2012). Nature and Story. *Go Into The Story*. https:// gointothestory.blcklst.com/patterns-nature-and-story-180bba5466f0.

[34] Leary, C. (2019). How the Golden Ratio Manifests in Nature. *Treehugger*. https://www.treehugger.com/how-golden-ratio-manifests-nature-4869736.

[35] Nargi, L. (2020). 30 Photos of the Rarest Animals on Earth. *Reader's Digest*. https://www.rd.com/list/rarest-animals-on-earth/.

[36] Mongoven, C. (2010). A style of music characterized by fibonacci and the golden ratio. *Congressus Numerantium*, 201, pp.127–138.

[37] Zahed, H. (2012). The Apple Logo. *Hzahed*, https://www.hzahed.com/post/The-Apple-Logo.

[38] Pokojski, W., Pokojska, P. (2018). Voronoi diagrams–inventor, method, applications. *Polish Cartographical Review*, 50, pp. 141–150, http://doi.org/10.2478/pcr-2018-0009.

[39] Babes-Bolyai Tudományegyetem. Algoritmikus geometria, 2003.

[40] Selimovic´, F., Stanimirovic´, P., Sarac˘evic´, M., Selimi, A., Krtolica, P. (2020). Authentication Based on the Image Encryption using Delaunay Triangulation and Catalan Objects. *Acta Polytechnica Hungarica*, 17, pp. 207–224, http://doi.org/10.12700/APH.17.6.2020.6.12.

[41] Place, S. M. (2015). *Tessellation Patterns*. http://www.spacemakeplace.com/tessellation-patterns/.

[42] Sánchez, P. (2015). Returns clustering with k-Means algorithm. *QuantDare*, https://quantdare.com/k-means-algorithm/.

[43] Golli, A. (2010). *Voronoi-like shapes in nature. Genetic Algorithms and Evolutionary Computing in Architecture*. http://genetichouse.blogspot.com/2010/08/voronoi-like-shapes-in-nature.html.

[44] de Sousa, V. (2017). Interactive transmedia vs. voronoi diagram expressions. *The 2017 International Science Fiction Prototyping Conference*, European Technology Institute, pp. 13–18.

[45] D'Agostino, S. (2019). Voronoi Tessellations and Scutoids Are Everywhere. *Scientific American*, https://blogs.scientificamerican.com/observations/voronoi-tessellations-and-scutoids-are-everywhere/.

[46] Bazalo, F. (2020). *Can voronoi division of space be used to optimise programatic volumes, structure and the distribution of facilities*. http://fbazalo.weebly.com/parametric-shelter-development.html.

[47] Dobashi, Y., Haga, T., Johan, H., Nishita, T. (2002). A Method for Creating Mosaic Images Using Voronoi Diagrams. *Eurographics 2002*, Short Presentations. Eurographics Association, http://doi.org/10.2312/egs.20021036

[48] Levin, G. (2000). *Segmentation and Symptom*. https://flong.com/archive/projects/zoo/index.html.

[49] CNN (2011). *Stunning superyacht design inspired by nature's hidden patterns*. http://edition.cnn.com/2011/TECH/innovation/06/10/voronoi.concept.yacht/ index.html.

[50] Architekten, F. (2011). *Voronoi Chair*. https://franken-group.com/projects/voronoi-chair?color=6150.0.147.

[51] Turner, T. (2011). *Yacht for Entertaining. Yanko Design*. https://www.yankodesign.com/2011/04/15/yacht-for-entertaining/.

REVIEWING COMMITTEE

Responsible for the Publication: Prof. dr. Zita Horváth
Published by the Miskolc University Press under leadership of Attila Szendi
Responsible for duplication: Works manager: Erzsébet Pásztor
Editor: Dr. Ágnes Takács
Technical editor: Csilla Gramantik
Proofreader: Zoltán Juhász
Number of copies printed:
Put the Press in 2021
Number of permission: MERT – 2021 – 276 – ME
HU ISSN 1785-6892 in print
HU ISSN 2064-7522 online